Promise and reality of post-lithium-ion batteries with high energy densities

Jang Wook Choi[1] and Doron Aurbach[2]

Abstract | Energy density is the main property of rechargeable batteries that has driven the entire technology forward in past decades. Lithium-ion batteries (LIBs) now surpass other, previously competitive battery types (for example, lead–acid and nickel metal hydride) but still require extensive further improvement to, in particular, extend the operation hours of mobile IT devices and the driving mileages of all-electric vehicles. In this Review, we present a critical overview of a wide range of post-LIB materials and systems that could have a pivotal role in meeting such demands. We divide battery systems into two categories: near-term and long-term technologies. To provide a realistic and balanced perspective, we describe the operating principles and remaining issues of each post-LIB technology, and also evaluate these materials under commercial cell configurations.

What characteristics define a good rechargeable battery? Although properties such as rate capability, cost, cycle life and temperature tolerance must be taken into consideration in any evaluation of a rechargeable battery[1,2], it is the improvement in energy density that has primarily driven the overall technological progress over the past 150 years — from lead–acid cells in the 1850s, nickel–cadmium cells in the 1890s and nickel metal hydride cells in the 1960s to, finally, lithium-ion batteries (LIBs) in the present day.

In the current era of LIBs, there is an ever-growing demand for even higher energy densities to power mobile IT devices with increased power consumption and to extend the driving range of electric vehicles. The growth of the global electric vehicle market has been slower than initially predicted about 5 years ago[3], which reflects the challenge that the battery industry faces: customers react very sensitively to the driving range (and thus the energy density) and price of electric vehicles. Because the energy density of a rechargeable battery is determined mainly by the specific capacities and operating voltages of the anode and the cathode, active materials have been the main focus of research in recent years. Other cell components, including separators, binders, outer cases and, to some extent, the major components of the electrolyte solution (that is, solvent and salt), have little room for further improvement. In other words, a dramatic increase in the energy density requires new redox chemistries between charge-carrier ions and host materials beyond the conventional 'intercalation' mechanisms[4]. Intercalation-based materials have a relatively small number of crystallographic sites for storing charge-carrier ions, leading to limited energy densities. For this reason, the electrodes that operate on the basis of distinct solid-state reactions, such as alloying and conversion, or that use gas-phase reactants have encountered growing interest owing to the likelihood that they will surpass the energy densities of intercalation-based electrodes.

New chemistries for charge-carrier ion storage serve as the basis for 'beyond intercalation' or so-called post-LIBs[5–7]. The systems governed by these new chemistries offer higher theoretical energy densities, and this benefit is usually translated to, at least, the initial cycles in experimental testing. It is becoming increasingly evident that the short lifetime is a serious problem of post-LIB systems. Indeed, the main technological challenge associated with these systems is overcoming their inferior reversibility. The main factors responsible for the low reversibility are instabilities during the phase transition of active materials and/or uncontrolled reactions at the electrode/electrolyte interface[8]; this implies that the electrode structures and electrolyte solutions should be developed and optimized as integrated systems to enable the realization of post-LIBs.

In this Review, we discuss a wide range of promising post-LIBs, focusing on their advantages and remaining challenges with respect to their governing chemistries. To construct an organized portfolio, we classify them into two distinct categories: near-term and long-term technologies. Near-term technologies have already been partially introduced in commercial products or are expected to mature within the next 5 years, and long-term technologies require at least 5 more years of fundamental research to become commercially viable. One

[1]*Graduate School of Energy, Environment, Water, and Sustainability (EEWS) and KAIST Institute NanoCentury, Korea Advanced Institute of Science and Technology (KAIST), 291 Daehak-ro, Yuseong-gu, Daejeon 305–701, Republic of Korea.*
[2]*Department of Chemistry and Bar-Ilan Institute of Nanotechnology and Advanced Materials, Bar-Ilan University, Ramat-Gan 5290002, Israel.*
jangwookchoi@kaist.ac.kr; Doron.Aurbach@biu.ac.il

Article number: 16013
doi:10.1038/natrevmats.2016.13
Published online 31 Mar 2016

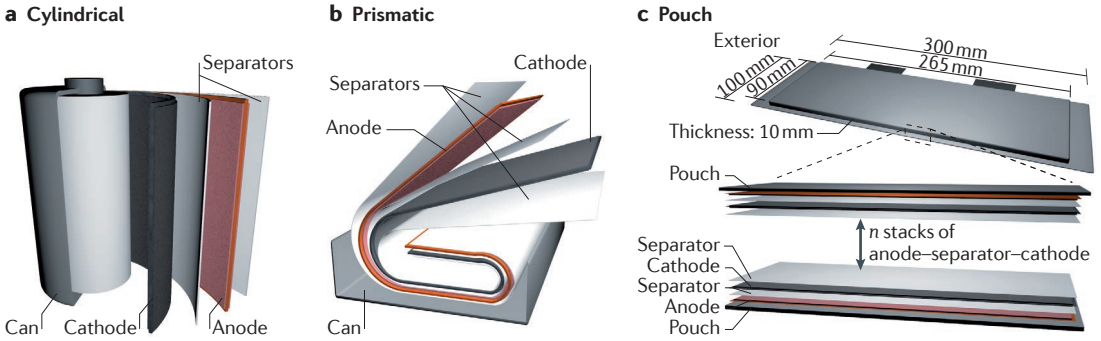

Figure 1 | **Three representative commercial cell structures. a** | Cylindrical-type cell. **b** | Prismatic-type cell. **c** | Pouch-type cell. The pouch dimensions are denoted, along with the internal configuration for *n* anode–separator–cathode stacks. Images are based on cells provided by SK Innovation.

of the main purposes of this Review is to draw a realistic and critical picture of the extent to which the energy density in commercial cells can be improved through the use of post-LIBs compared with existing LIBs. This analysis is important because the energy-density evaluations presented in many previous literature sources are based on gravimetric capacities of active materials that exclude other dead-volume and dead-weight components, and therefore overestimate the energy densities of post-LIBs[9]. Rather than detail all advancements for each class of post-LIB, we focus on crucial technological issues that may have a strong impact on the practical energy densities of these systems.

Commercial cell configurations

Before addressing each of the various post-LIBs, we first discuss the different structures of commercial cells. In large-scale applications (for example, in electric vehicles), a certain number of cells are packed into a module. The design of the modules depends largely on the size and shape of the products, as well as their interconnecting circuits, safety and temperature control aspects. We restrict the scope of this Review to the material properties and behaviour at the single-cell level.

Current commercial cells adopt three cell types: cylindrical, prismatic and pouch (FIG. 1). Cylindrical cells in most products (including those used for Tesla Motors' vehicles) follow a standard model in terms of size — namely, the 18650 cell. Typical 18650 cells in commercial LIB products hold volumetric energy densities of 600–650 Wh l^{-1}, which are ~20% higher than those of their prismatic and pouch counterparts[10,11] because a stacked cell assembly in a cylindrical cell is wound with a higher tension. The energy density of battery systems can be compared on a gravimetric or volumetric basis. It seems that for many practical systems, the volumetric aspect is more important, because most battery packs are designed according to the available volume. Despite the higher energy densities of cylindrical cells, prismatic and pouch cells are adopted for a wide range of applications owing to their smaller dead volumes on the module level and higher degrees of design freedom; in contrast to cylindrical cells, the size of prismatic and pouch cells is easily customized for the final product. Hence, we took the pouch cell as a common platform to examine the volumetric energy densities of selected battery systems and used the specific volumetric energy densities as the basis for comparison.

As depicted in FIG. 1c, fixed dimensions of 300 mm (length) × 100 mm (width) × 10 mm (thickness) are used by benchmarking a product of one battery manufacturer (SK Innovation). Inside this prototype cell, *n* anode–separator–cathode stacks are incorporated to occupy the given pouch thickness, with both sides of each current collector, except the outermost stacks, coated with electrode films. In this commercial pouch setting, a conventional $LiCoO_2$–graphite cell delivers 491 Wh l^{-1} (Supplementary information S1 (table)), which is in the range of many current commercial products. We evaluated other post-LIBs under an identical cell configuration.

Near-term technologies

The active materials in this category of post-LIBs have been developed to a level that enables their partial use in the electrodes of current commercial products. Research on these active materials is ongoing to increase their content in the electrodes of the corresponding post-LIB cells.

Silicon anodes. Natural and artificial graphite have long been the main anode-active materials in LIBs[12,13] and serve as a universal reference in evaluating new materials. Among many higher-specific-capacity alternatives to graphite that are under investigation, Si is one of the most promising anode materials because of its superior theoretical capacity (>4,000 mAh g^{-1}) and attractive operating voltage (~0.3 V versus Li/Li^+)[14–17]. Since the early work conducted at Argonne National Laboratory[18] and General Motors[19,20] in the 1970s, considerable research efforts have focused on overcoming the key failure modes in the cyclability that originate from the huge volume change of Si upon lithiation–delithiation (FIG. 2a). Progress in this area has been made using smart electrode structures[21–26] and binder designs[27–37], whereby the issues of pulverization of the active material and peeling-off of the electrode active mass can be simultaneously resolved. Another critical problem of Si electrodes is the formation of unstable passivation layers. In practice, when the

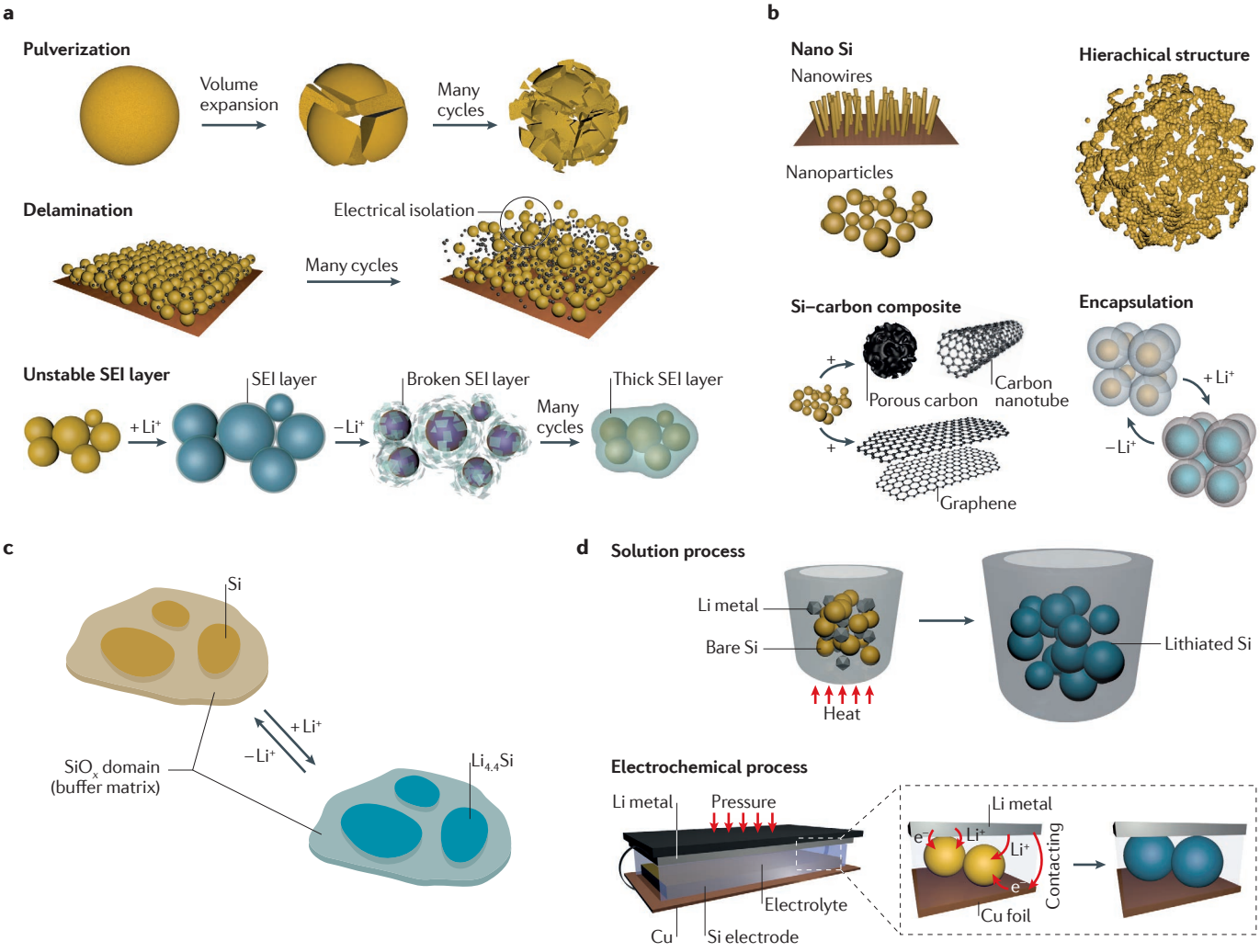

Figure 2 | **Electrode structures and binder designs for Si anodes. a** | Main degradation mechanisms of Si anodes originating from the large volume expansion of Si during lithiation. **b** | Various morphologies of Si-active materials and their composites. **c** | Reversible lithiation–delithiation process of SiO_x. **d** | Prelithiation of Si anodes via a solution process and an electrochemical process. **e** | Various binder concepts for Si anodes. SEI, solid electrolyte interphase.

electrode volume fluctuates drastically, it is very difficult to develop a stable solid electrolyte interphase (SEI), which serves as a protecting film on the electrode surface. This interfacial issue can be largely resolved by a judicious selection of electrolyte solution[38–41].

From the viewpoint of electrode structure, composites[21–26] that buffer the volume expansion of Si through conductive nanoporous structures are remarkable; they demonstrate greatly enhanced cyclability compared with those simply based on bare Si nanomaterials. These composite components include porous carbon[21,24,25], graphene[26], tubular templates[23] and other semiconducting materials[22] with similar morphologies (FIG. 2b). Despite the significantly improved cyclability based on these structural designs, the industry has instead adopted the silicon monoxide phase (SiO_x, $x \approx 1$) as the first Si-based commercial anode material (FIG. 2c), because these materials can be produced in massive

quantities in both gas-phase[42,43] and solution-based[44] processes, and are also available at a reasonable price (approximately US$100 per kg versus $10–20 per kg of graphite) and with reliable quality. However, SiO_x is used in a blended form with graphite, but its content is typically less than 5 wt%, which reflects the infancy of Si anode technology. The main challenge associated with SiO_x is its poor initial Coulombic efficiency (ICE), which reaches only 50–60%[45] without a carbon surface coating. This low efficiency leads to an excessive loading of the cathode material and, therefore, to a sacrifice in the energy density of the entire cell. A more fundamental difficulty in designing an active Si structure is simultaneously attaining long-term cyclability and high ICE, because these two attributes require contradictory material features: the buffering matrices and porous structures implemented to accommodate the volume change of Si and thus achieve long-term cyclability are detrimental to the ICE because of increased Li-ion trapping and interfacial reactions. In this context, recent attempts to prelithiate Si-containing anodes using solution[46] or electrochemical processes[47,48] (FIG. 2d) could become very useful. Such approaches orthogonally address the ICE problem without impairing the long-term cyclability.

Polymeric binders have proved to be effective in enhancing the cyclability of Si electrodes. Conventional polyvinylidene difluoride (PVDF) has been replaced by new binders (FIG. 2e), such as polymers with crosslinked chains[27,28], self-healing polymeric matrices[29,30], carbohydrate-based polymers[31–35] and electronically conducting polymers[36,37]. These new binders are effective in maintaining the electrode structure during the repeated volume change of Si, mainly via 3D interchain interactions. The remaining objectives in binder research are: first, to preserve the new binder functions at a lower binder content comparable to the present industrial conditions (<5 wt%); second, to develop hybrid polymers that bind Si and graphite (or other carbonaceous materials) simultaneously; and, last, to optimize binder functionalities in such a way that the binding affinity with Si is increased, but Li-ion trapping is minimized for high Coulombic efficiency. In particular, supramolecular chemistry that can incorporate non-covalent interactions (such as hydrogen bonding, ion–dipole and π–π interactions) is expected to be a useful tool in tuning network properties between polymers and active particles[28].

Using the pouch cell configuration in FIG. 1c and pairing it with $LiNi_{0.8}Co_{0.1}Mn_{0.1}O_2$ electrodes as representative high-capacity cathodes (see the next section), a 50% replacement of graphite with a commercial SiO_x is predicted to increase the energy density by 7.6%, from 513 Wh l^{-1} (Supplementary information S2 (table)) to 552 Wh l^{-1} (Supplementary information S3 (table)), when 110% swelling (the average observed[49,50] value between graphite and SiO_x) is postulated for the composite anodes. Prelithiation of SiO_x may increase the energy density further to 628 Wh l^{-1} (Supplementary information S4 (table)) through lowering the cathode loading by balancing the capacities of both electrodes. If only 50% swelling is assumed, the energy density of cells with prelithiated SiO_x-based anodes can increase further to 710 Wh l^{-1} (Supplementary information S4 (table)). These comparative energy-density values demonstrate that achieving high ICE and suppressing electrode swelling are very important for utilizing the high intrinsic capacity of Si to attain high volumetric energy density.

Layered nickel-rich and lithium- and manganese-rich cathode materials. The next emerging cathode materials in the field of LIBs are Ni-rich and Li- and Mn-rich layered materials, the origins of which can be traced to the early works by the Dahn[51] and Thackeray[52] groups, respectively. They are the successive generation of their long-standing layered counterparts, $LiCoO_2$ (~145 mAh g^{-1}) and $LiNi_{1/3}Co_{1/3}Mn_{1/3}O_2$ (~153 mAh g^{-1})[53]. In fact, Ni-rich materials are already partially included in commercial products[54], with $LiNi_{0.8}Co_{0.15}Al_{0.05}O_2$ being a representative example[55]. In addition, on the basis that layered transition metal (TM) oxides with Mn have advantages in terms of safety and rate capability, there have been attempts[56] to develop Ni-rich $LiNi_xMn_yCo_zO_2$ ($x+y+z=1$) layered cathode materials in which $x>0.6$. All of these layered materials have a common host structure in which Li and TM slabs are alternately repeated in the overall cubic close-packed (ccp) frame of O atoms, and Li and TM ions are positioned at the octahedral sites in the corresponding slabs (FIG. 3a). In addition to this underlying host structure, in the Ni-rich and Li- and Mn-rich phases, there is well-known Li–TM mixing and secondary phases scattered throughout each particle, respectively (FIG. 3a, right). Compared with their conventional layered analogues, the Ni-rich phases raise the specific capacity owing to their electronic structures, as with $LiNiO_2$; in contrast to $LiCoO_2$, the e_g energy band of $LiNiO_2$ does not overlap with the O_{2p} band[57], allowing a higher degree of charging without perturbing the O_2 framework. In the case of Li- and Mn-rich phases, the increased capacity originates from the presence of Li_2MnO_3 (in addition to an active $LiMO_2$ layered phase), which is activated in the first charge during Li extraction and O_2 evolution[58]. This activation, achieved at a potential of >4.7 V, can provide Li- and Mn-rich layered cathode materials with a gravimetric capacity higher than 250 mAh g^{-1}. The representative voltage profiles in the first cycle for these two types of material[59,60] are displayed in FIG. 3b.

Despite their enhanced capacity, these two emerging layered materials often encounter capacity fading during cycling, arising mainly from common detrimental structural and surface changes. Upon Li-ion extraction during charging, both layered materials tend to transform to the more thermodynamically stable spinel-like phases[56]. Crystallographically, this spontaneous transition is initiated by the preferential migration of TMs to the octahedral sites in the Li slabs (also known as Li–TM mixing; FIG. 3c) and results in a drop in both the voltage profile[61] (FIG. 3d) and the capacity during discharge. The structural instability is also caused by an unstable interface; TMs from the Ni-rich and Li- and Mn-rich phases are known to dissolve[57], generating irreversible and inactive interfacial compounds. In addition, the surface interactions of these nucleophilic and basic

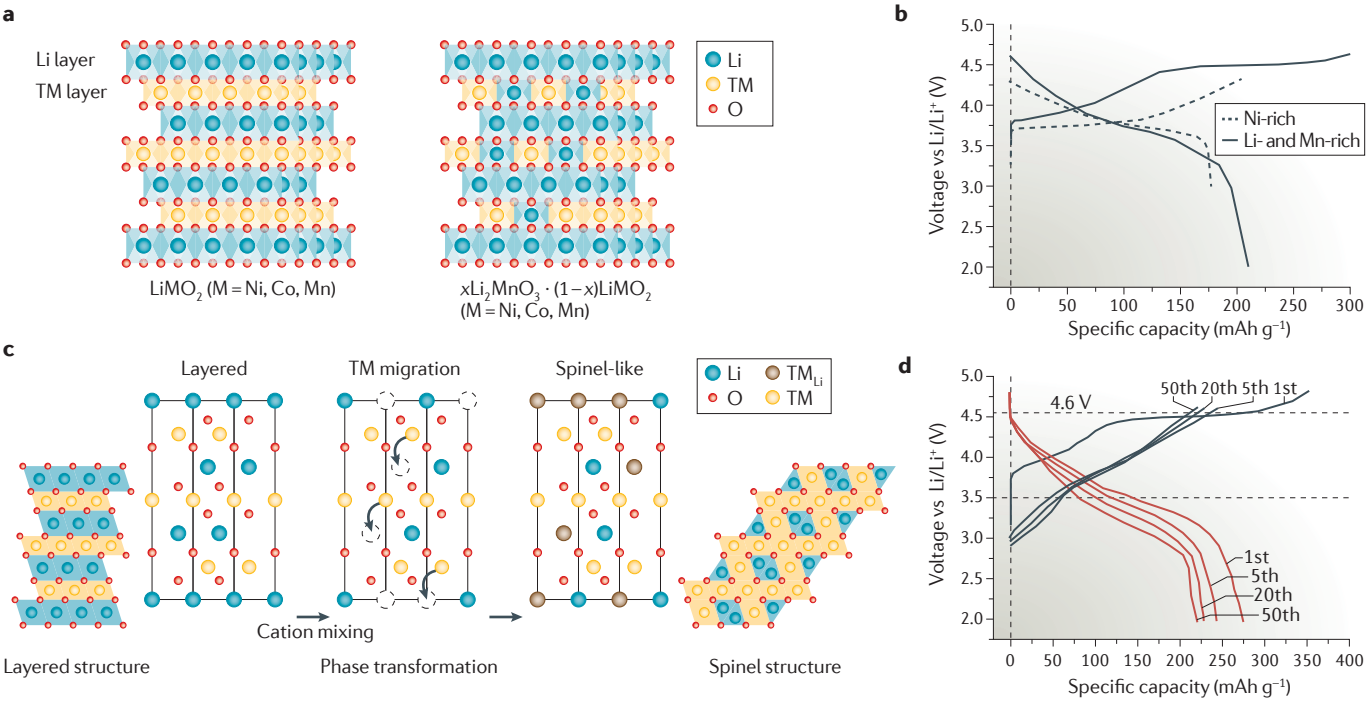

Figure 3 | **Structures and electrochemical voltage profiles of advanced layered cathode materials. a** | Crystal structures of $LiMO_2$ (M = Ni, Co or Mn) and its Li- and Mn-rich derivative xLi_2MnO_2–$(1-x)LiMO_2$ (M = Ni, Co or Mn). **b** | Voltage profiles of a $Li/Li[Ni_{0.6}Co_{0.2}Mn_{0.2}]O_2$ cell and a $Li/0.3Li_2MnO_3 \cdot 0.7Li[Ni_{1/3}Co_{1/3}Mn_{1/3}]O_2$ cell cycled between 3.0 and 4.3 V, and 2.0 and 4.6 V, respectively, at room temperature. **c** | Layered-to-spinel transformation upon charging. **d** | Voltage profile for the continued cycling between 2.0 and 4.6 V in a Li- and Mn-rich cathode material $(xLi[Li_{1/3}Mn_{2/3}]O_2 \cdot (1-x)LiMn_{1/3}Ni_{1/3}Co_{1/3}O_2$ (x = 0.6)) owing to the layered-to-spinel transition. TM, transition metal. Panel **b** is adapted with permission from REF. 59, American Chemical Society; and is adapted from REF. 60, reproduced by permission of the Electrochemical Society. Panel **d** is adapted from REF. 61, reproduced by permission of the Electrochemical Society.

cathode materials with solution species (acidic moieties such as HF, PF_5 and electrophilic alkyl carbonates) form resistive surface films that increase the electrode impedance[62]. Some strategies, including TM doping[63–65], surface coating with AlF_3 (REF. 66), Al_2O_3 (REFS 67,68), $AlPO_4$ (REFS 69,70), carbon[71] and TiO_2 (REFS 72,73), implementation of spinel phases near the surface region[74,75] and the incorporation of concentration gradient structures[76], have been reported to be effective in addressing the failure mechanisms. Nonetheless, research is expected to continue in the pursuit of more robust solutions, but progress may not be easy because performance fading originates from thermodynamically favoured phase-transition processes. Between these two classes of layered materials, realistic solutions based on cost-effective approaches are less available for Li- and Mn-rich layered materials, leading to relatively slower progress towards commercialization.

With graphite used as an anode-active material, the replacement of traditional $LiCoO_2$ with $LiNi_{0.8}Co_{0.1}Mn_{0.1}O_2$ or $Li_{1.19}Mn_{0.54}Ni_{0.13}Co_{0.12}Ru_{0.01}O_2$ results in a moderate increase in energy density from 491 Wh l^{-1} to 513 and 524 Wh l^{-1} (4.4% and 6.7% increases), respectively (Supplementary information S1,S2 (tables); Supplementary information S5 (table)). The increase in volumetric energy density is smaller than expected based on the higher gravimetric capacity of these materials owing to the lower density (3.0–3.3 g cm^{-3} versus 4.0 g cm^{-3} for $LiCoO_2$) of active material in the fabricated electrodes. This result guides us towards another useful research direction for Ni-rich and Li- and Mn-rich cathode materials: increasing the density of the active powder and the electrode film. In addition, the volumetric energy density increases to 552 and 661 Wh l^{-1}, respectively, when 50 wt% of graphite is replaced by SiO_x (Supplementary information S1–S3,S5 (tables); Supplementary information S6 (table)).

Long-term technologies

The active materials in this category of post-LIBs have the potential to increase the energy density more significantly. However, their reversible operation, which is essential for long-term cyclability, is not fully guaranteed and requires fundamental research to understand the properties and behaviour of the electrodes and electrode/electrolyte interfaces.

The lithium-metal anode. Since Whittingham *et al.*[77] demonstrated the Li–TiS_2 system, Li metal has been considered as one of the most ideal anodes in LIBs owing to its high theoretical capacity (3,860 mAh g^{-1}) and low redox potential[78,79]. However, severe surface dendrite formation causes poor interfacial stability and safety issues. More than 15 years ago, it was concluded that Li metal was not a suitable anode material in rechargeable batteries[80]. Nevertheless, in recent

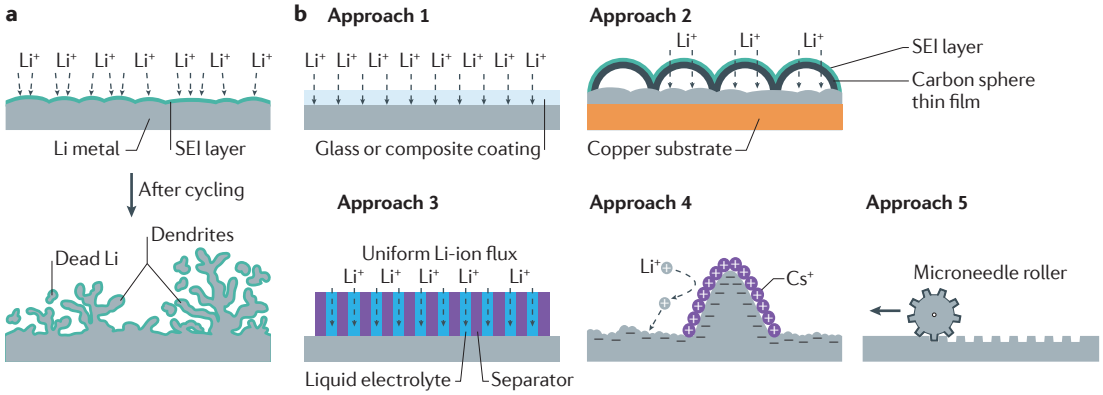

Figure 4 | **Failure and remedies of Li-metal anodes. a** | Failure mechanism of Li-metal anodes. **b** | Approaches to minimize Li-dendrite growth and improve the interfacial stability: approach 1, surface coating with glass or composite; approach 2, surface coating with thin carbon or graphene layers; approach 3, uniform Li-ion flux; approach 4, adding Cs^+ to the electrolyte; approach 5, incorporating 3D patterns or using Li-metal powder. SEI, solid electrolyte interphase.

years, the community has seen a renaissance in research and development efforts aimed at using metallic Li in high-energy-density rechargeable batteries. Dendrite growth is very difficult to prevent because it can be initiated from nanoscale roughness on the surface; incoming Li ions are preferentially deposited at relatively sharp tips and protruding morphologies of the innate Li-metal surface (FIG. 4a). Various coating materials, including glasses[81,82] and composites[83] (approach 1 in FIG. 4b) were reported to suppress dendrite growth to a great extent by exerting pressure against the surface and blocking the space that is open for further dendrite growth. As a distinct coating scheme, thin carbon[84] and graphene layers[85] that separate SEI layers from dendrite growth have recently been reported to improve charge–discharge efficiency by restricting electrolyte decomposition above the coating layers (approach 2 in FIG. 4b). Other approaches[86,87] have also been developed to make Li-ion flux more uniform over the Li-metal surface (approach 3 in FIG. 4b), because uniform flux can prevent local increases in Li-ion concentration, which is essential for dendrite growth. Coating the separators with materials that possess good wetting capability (by the electrolyte solutions) is a well-known strategy in this direction[86]. Electrolyte solutions containing functional additives have also proved to be effective. In addition to small-molecule-based additives[88–90], additives that function on the basis of electrostatic interactions with Li ions were recently discovered[91]; Cs^+ ions at low concentrations (approach 4 in FIG. 4b) remain positively charged and repel incoming Li ions from sharp tips, which causes the surface morphology to be more rounded. Finally, strategies (approach 5 in FIG. 4b) that incorporate 3D patterning[92] or use Li-metal powder[93] are also valid, because the increased effective surface area by the 3D morphology dissipates the electron density at the given areal current density.

To evaluate the volumetric energy density, cases with and without the swelling of the Li-metal anode were considered (Supplementary information S7 (table); Supplementary information S8 (table)). The separator thickness was also varied to include reasonable amounts of extra electrolyte solution, because it is essential to compensate for the consumption of the electrolyte solution at the Li-metal interface. When 100% swelling is assumed, the energy density ranges from 650 to 764 Wh l^{-1} upon pairing with $LiNi_{0.8}Co_{0.1}Mn_{0.1}O_2$ (Supplementary information S7 (table)), corresponding to a 32.0–55.6% improvement compared with the $LiCoO_2$–graphite reference. These values rise further to 743–890 Wh l^{-1} (Supplementary information S8 (table)) if no swelling is assumed for the Li-metal anode, which demonstrates that stabilizing the Li-metal anode interface can considerably improve the energy density. Despite these promising energy densities, the commercial success of Li-metal anodes is still not guaranteed because none of the existing solutions meets the commercial standards in terms of electrochemical performance and large-scale processing.

Lithium–sulfur batteries. Sulfur is one of the most promising active materials because of its high theoretical capacity (1,675 mAh g^{-1}), low cost and natural abundance. Li–S batteries were first conceptualized[94] by Mallory P. R. & Co in the 1960s and electrochemically demonstrated by Rauh *et al.*[95] in the 1970s but were later abandoned. Intensive research and development was recently renewed because of the increasing demand for high-energy-density power sources[96–99]. Indeed, following the initial commercial effort by Poly Plus, Sion Power Corporation has launched commercial Li–S products targeting unmanned vehicle systems and military communication applications. Remarkably, the problem of polysulfide dissolution into most electrolytes, which leads to a shuttling process involving the Li-metal anode, has been largely addressed using two approaches.

The first approach is to passivate the Li-metal anode using electrolyte solutions containing active agents, such as lithium nitrate ($LiNO_3$), which react on the Li-metal anode to form a film on the surface that blocks facile electron transfer[97]. The second approach is to use smart composite electrode structures in which elemental sulfur is encapsulated by conductive porous materials and

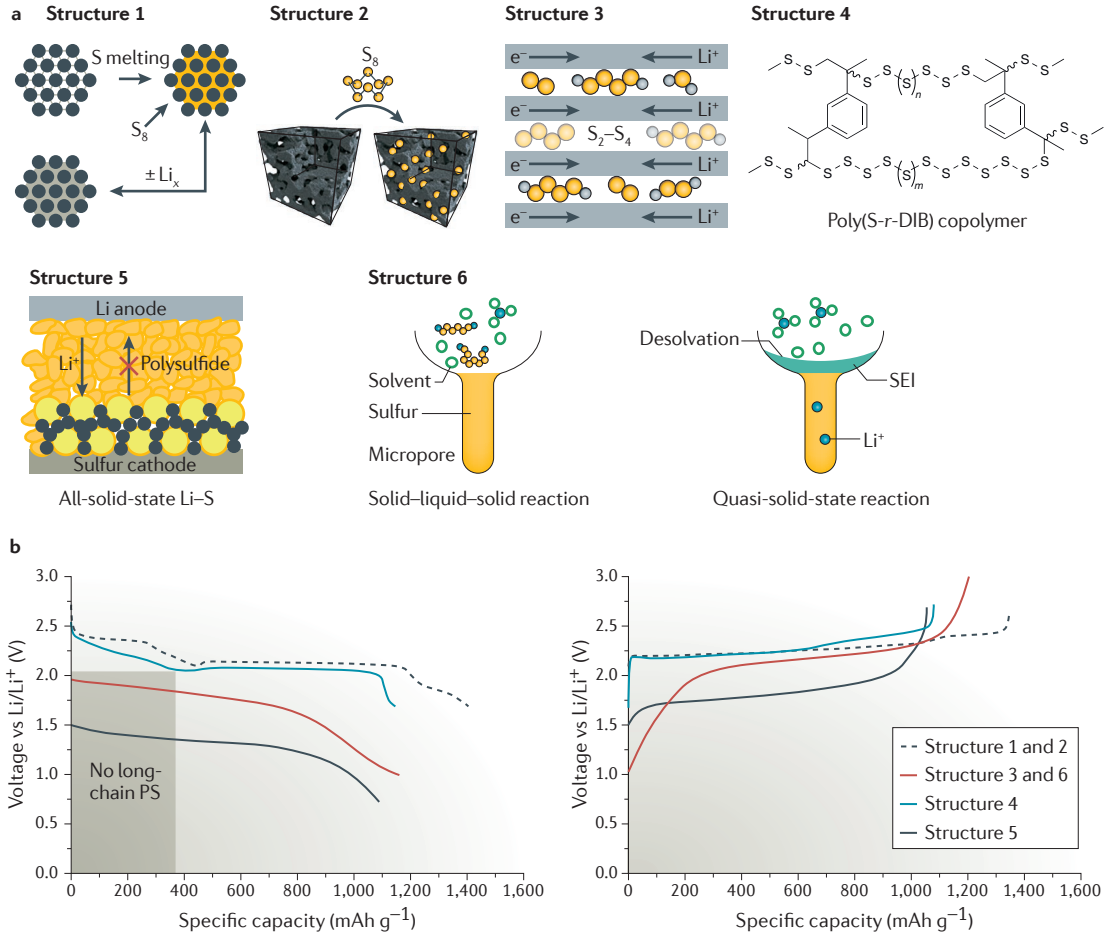

Figure 5 | **Various sulfur cathodes in Li–S batteries. a** | Schematic illustration of representative electrode structures: structure 1, sulfur encapsulated by conductive porous materials or nanoassemblies; structure 2, sulfur encapsulated in activated carbon fibres; structure 3, sulfur confined in small pores; structure 4, sulfur conjugated to polymer backbones or organic moieties; structure 5, using solid or solid-like electrolytes; structure 6, developing a solid electrolyte interphase (SEI) protecting film. **b** | Corresponding discharge–charge (left and right panels, respectively) profiles of the structures in panel **a**. Poly(S-r-DIB), poly(sulfur-random-1,3-diisopropenylbenzene); PS, polysulfide.

nanoassemblies[100] (structure 1 in FIG. 5). Effective sulfur–carbon cathodes have been demonstrated in which sulfur is encapsulated in activated carbon fibres (structure 2 in FIG. 5)[101]. These two approaches also resolve the issue of the poor electronic conductivity (~10^{-30} S cm^{-1}) of sulfur. The incorporation of metal oxides[102] and nitrogen doping[103] in carbon backbones provide additional help for suppressing polysulfide dissolution because they have atomic configurations that enable a strong binding affinity to lithium polysulfides. In addition to simple encapsulating structures, polysulfide dissolution can be circumvented using chemical approaches; sulfur can exist in the form of short linear chains when confined in small pores[104] (structure 3 in FIG. 5), or conjugated to polymer backbones[105] or organic moieties[106] (structure 4 in FIG. 5). Soluble long-chain polysulfides can also be avoided by using solid[107–111] or solid-like[112–115] electrolytes (structure 5 in FIG. 5), because the formation of the long-chain polysulfides is accompanied by the dissolution of S_8 at the solid/liquid biphasic interface[116], which is absent in solid electrolytes. The disappearance of the high-voltage plateau near 2.4 V in structures 3–5 in FIG. 5 is another indication of the elimination of soluble long-chain polysulfides.

In addition to the structures described above, great interest lies in encapsulating sulfur at high content (>60 wt%) in activated carbons possessing wide pores to form an SEI-type protecting film on the surface of the composite sulfur–carbon cathodes[117,118], as is schematically shown in structure 6 in FIG. 5. Using this approach, all redox reactions of the sulfur cathodes take place in a quasi-solid manner confined in the composite structure. The detrimental shuttle mechanism is thereby avoided, and it is possible to even use electrophilic carbonate solutions.

The energy density of Li–S cells should be carefully assessed, because their volumetric energy density is often neglected to emphasize the superior gravimetric capacity of sulfur. When free-standing carbon nanotube–sulfur electrodes[119] (with a sulfur content of 54 wt%) are used as prototypes and the excess Li amount in the anodes is varied from 0% to 100% in terms of the capacity, the energy

density ranges from 283 to 314 Wh l^{-1} (Supplementary information S9 (table)), which, surprisingly, is even smaller than that of $LiCoO_2$–graphite LIBs (Supplementary information S1 (table)). These values, which were smaller than expected, are attributed to the low electrode density of most plausible composite sulfur electrodes, which leads to a relatively small stack number within a given volume. If we consider a case in which sulfur occupies 80 wt% of the electrode without a binder and void space, the theoretical energy density of the full cell can reach 867 Wh l^{-1} without an excess of Li; this reconfirms the importance of densifying composite sulfur electrodes for practical use. This evaluation demonstrates that for Li–S cells to be competitive, strategies to increase the sulfur-cathode density, such as roll pressing and high-content sulfur design, are crucial. Thus, future research should be aimed at developing high-density electrode designs that simultaneously alleviate polysulfide dissolution. The reversibility of the Li-metal anode also has an important role, because it is desirable to minimize excess Li loading. Even with the aforementioned advanced approaches, using Li anodes is still likely to significantly limit the cycle lives of practical batteries. Alternative strategies for replacing Li metal with more reversible anodes, such as hard carbons or Si, would, in turn, sacrifice the energy density considerably. Hence, Li–S batteries may be better targeted to specific applications for which gravimetric-specific energy is critical and limited cyclability is tolerable. In addition to improving the energy density and cycling performance, certain processing issues for large-scale manufacturing need to be carefully addressed. In particular, ether-based solvents that are highly volatile could make it difficult to maintain a constant viscosity of the slurry throughout processing. In this regard, less volatile solvents are preferable and are a good direction for future research.

Metal–oxygen battery systems. Secondary Li–O_2 batteries were first demonstrated by Abraham *et al.*[120] in the 1990s, and Zn–O_2 batteries were developed[121,122] earlier, in the 1970s. The use of O_2 molecules from the air as an active material, instead of solid materials, promises a drastic improvement in the energy density, which has renewed interest in this direction. However, poor reversibility remains a problem in most metal–oxygen cells, and the charge–discharge efficiency in each cycle and long-term cyclability in most cells are far inferior to those of LIBs. Both Li–O_2 and Zn–O_2 systems share the same drawbacks: irreversible discharge products, electrolyte evaporation, and water and oxygen attack at the metal surface.

Li–O_2 cells operate in both aqueous and non-aqueous electrolytes on the basis of two governing reactions[5,120,123]: $2Li^+ + 2e^- + 1/2O_2 + H_2O \rightarrow 2LiOH$, 3.45 V (aqueous) and $2Li^+ + 2e^- + O_2 \rightarrow Li_2O_2$, 2.96 V (non-aqueous). In the aqueous operation (FIG. 6a), the discharging process produces a soluble product, LiOH, which prevents the air cathode from clogging and reaching high overpotentials. However, LiOH does not readily decompose during charging and can also precipitate[5,123] above ~5 M, which impairs the energy density and cyclability. More importantly, the incompatibility of aqueous media with Li metal requires a surface coating[5,124] of, for example, LISICON ($LiM_2(PO_4)_3$, $Li_{1+x+y}Al_xTi_{2-x}Si_yP_{3-y}O_{12}$)[5,124–127]. Moreover, the surface-coating layers do not usually provide long-term protection from Li-dendrite formation and pH variation, and eventually lead to a rate-performance penalty[123]. Because of these fundamental and technical reasons, more attention has been directed to non-aqueous Li–O_2 cells (FIG. 6b) in recent years.

A major challenge for non-aqueous Li–O_2 cells lies in improving the reversibility in each cycle. To achieve this, two main approaches are applied: first, increasing the decomposition efficiency of the main discharge product[123,128], Li_2O_2; and, second, avoiding unwanted side reactions[5,129–131], which give rise to compounds that reduce the reversibility. In the early stages of research using the first approach, the community concentrated on the development of cathode catalysts with diverse metal[128,132–135] and metal-oxide[136–138] nanostructures. However, identifying functional catalysts remains a challenge, and their effects are easily concealed because the charging efficiency is largely affected by the preceding discharging products and conditions[139–141]; that is, the amount of side products, crystallinity and morphology of Li_2O_2, the degree of discharge and the current density.

In addition to cathode catalysts positioned inside the electrodes, a new concept of a redox mediator[142,143] — a so-called soluble catalyst — dissolved in the electrolyte was introduced to increase the Li_2O_2 decomposition efficiency. By utilizing its soluble nature, a redox mediator undergoes charge transfer efficiently with conductive electrode surfaces and re-transfers the charge from Li_2O_2, improving the electron transport from Li_2O_2 that would otherwise be hindered because of the low electronic conductivity of Li_2O_2.

Meanwhile, recent investigations[5,129,140,144,145] have revealed that, regardless of the solvent used in the electrolyte, most non-aqueous Li–O_2 cells suffer from electrolyte decomposition, which generates side products (for example, Li_2CO_3, HCO_2Li and CH_3CO_2Li) with poor reversibility. Although the formation of side products occurs in all solvents, it is less severe in ether-based cells than in carbonate-based ones[129,144]. In a recent series of papers[146–149], it was demonstrated that all relevant non-aqueous solvents are reactive towards basic and nucleophilic O_2 reduction products (that is, superoxide and peroxide moieties) in the solution phase containing highly electrophilic Li ions. We note that all carbonaceous electrode materials can degrade by reacting with superoxide and peroxide moieties. As a result, the research focus has turned to minimizing side reactions, driving the community to use non-carbonaceous electrode materials (such as Au (REF. 132), TiC (REF. 150), Ti_4O_7 (REF. 151), Co_3O_4 (REF. 152), Mo_2C (REF. 153) and RuO_2 (REF. 154)) and carefully select the electrolyte solutions[129,140,145,155].

Despite the long history of primary Zn–O_2 batteries in hearing aids, navigation lights, remote communications and railway signal amplifiers, secondary Zn–O_2 batteries are still at the research stage. Compared with Li–O_2 cells, secondary Zn–O_2 cells deliver lower

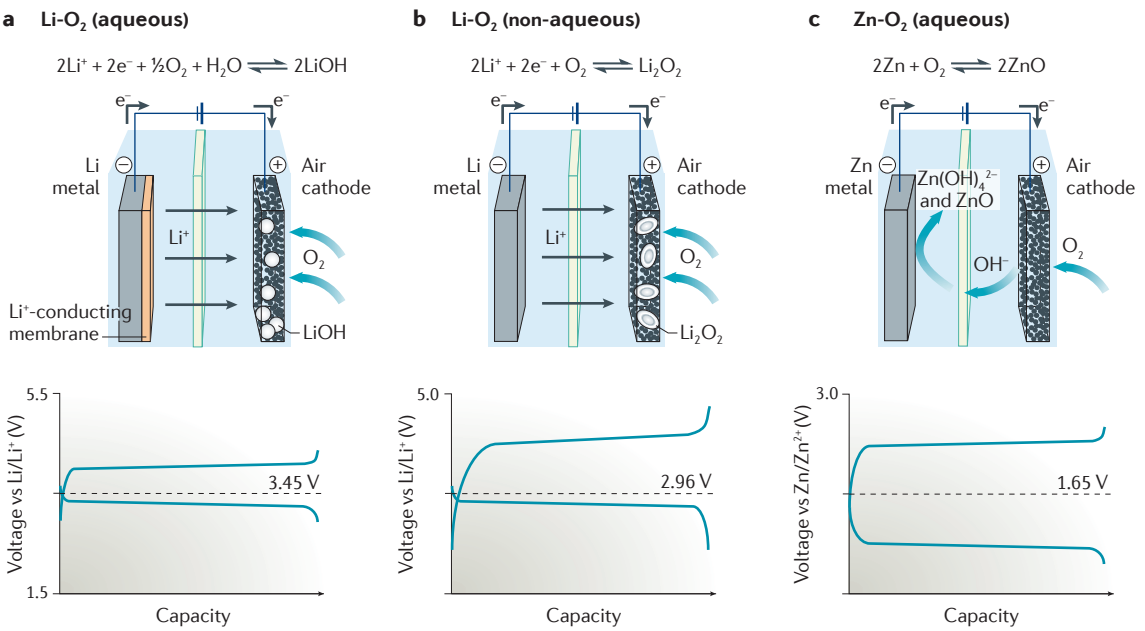

d

Component	Li-O_2(aqueous)	Li-O_2(non-aqueous)	Zn-O_2(aqueous)
Cathode	• Requires gas separation membrane • Requires ORR or OER catalysts • LiOH and Li_2CO_3 precipitation	• Requires gas separation membrane • Requires ORR or OER catalysts • Carbon decomposition over 3.5 V • Pore clogging by reaction products	• Requires gas separation membrane • Requires ORR or OER catalysts • Electrode peel-off • Pore clogging by carbonates
Anode	• Requires Li^+-conducting membrane • Safety issue • LiOH precipitation • Dendrite formation	• Corrosion by water and crossover O_2 • Dendrite formation	• Dendrite formation • ZnO passivation • H_2 evolution by Zn corrosion
Electrolyte	• Limited LiOH solubility • Evaporation	• Oxidation at high voltages • Vulnerable to O_2^- attack • Evaporation	• Evaporation and water electrolysis • Carbonate formation by reaction with CO_2

Figure 6 | **Representative metal–oxygen batteries. a–c** | Governing reactions, cell configurations and charge–discharge profiles for Li–O_2 (aqueous and non-aqueous) (panels **a** and **b,** respectively) and Zn–O_2 batteries (panel **c**). **d** | The challenges faced in the development of the cathode, anode and electrolyte of each battery from panels **a**–**c**. OER, oxygen evolution reaction; ORR, oxygen reduction reaction.

gravimetric energy densities[156], although decent cyclability was recently reported[121,157]. The lower gravimetric energy densities originate from the smaller gravimetric capacity of Zn than that of Li, as well as the lower operating cell voltages (~1.65 V) due to the limited potential windows of aqueous electrolytes. Nonetheless, the use of Zn and aqueous electrolytes provides advantages of being low cost, environmentally benign and having high rate capability. More importantly, Zn–O_2 batteries can offer promising volumetric energy densities. As shown in FIG. 6c, the governing reaction comprises a discharging reaction at the anode that involves OH^- ions forming the soluble zincate ($Zn(OH)_4^{2-}$) anion and the reduction of O_2 to soluble OH^- at the cathode[121,156]. Thus, in contrast to Li–O_2 cells, the discharge products on the cathodes of Zn–O_2 cells are mostly soluble, which makes the cathodes more reversible upon charging. The remaining challenges to meet commercial standards in terms of cyclability and rate capability are: to minimize ZnO passivation[121,158,159] on the Zn-anode surface and Zn-metal corrosion[121,160–163]; to develop effective oxygen evolution reaction (OER) and oxygen reduction reaction (ORR) catalysts[157,164]; and to prevent carbonate formation[121,165] from the reaction between CO_2 in air and KOH in the electrolyte.

The evaluation of the energy density of metal–oxygen batteries is not trivial even at the cell level, because the dimensions of the O_2 gas inlet and catalyst layer are not commercially standardized, which leads to considerable variation in the entire cell volume. We assume that O_2 gas flows through channels along each current collector with a thickness of 50 µm. In the case of Li–O_2 cells, when Super P powder is used as a main conductive component in air cathodes, with reversible capacities of 1,000 and 2,000 mAh g^{-1}, the cathode porosity is 78% and the energy density is 440 and 581 Wh l^{-1}, respectively (Supplementary information S10 (table)). Similarly, replacement of the Super P electrode with a Co_3O_4 catalyst electrode increases the energy density slightly to 536 and 659 Wh l^{-1}, respectively (Supplementary information S11 (table)). These values are smaller than the initial optimistic estimations and are ascribed to the volume occupation of the gas channels and the porosity

of the air cathodes. Despite the lower operating voltage, Zn–O_2 batteries could offer more promising volumetric energy densities because the liquid-based reaction can reduce the cathode volume. Assuming a catalyst layer with a thickness of between 1 and 10 μm, the energy density ranges from 487 to 502 Wh l^{-1} (Supplementary information S12 (table)) when the reversible capacity of Zn is limited at 100 mAh g^{-1}. The range rises dramatically to 1,468–1,582 Wh l^{-1} (Supplementary information S13 (table)) once the reversible capacity of Zn is set to 600 mAh g^{-1}, indicating that the reversible capacity of the Zn anode is very critical. Irrespective of the main reactions, the volumes required for gas flow and for the accommodation of reaction products in the cathode have a decisive role in determining the volumetric energy density, demonstrating the importance of having an air-cathode design that covers both the electrode layer and the gas channel. Owing to unsolved issues on both the material and cell levels, metal–oxygen batteries are unlikely to have a significant commercial impact in the near future.

Sodium-ion batteries. Because of the obvious advantages of the low cost and natural abundance of Na precursor materials, Na-ion batteries (SIBs) have been investigated for grid-scale energy storage systems[166]. The size of the global rechargeable battery market is predicted to grow from about $10 billion in 2010 to over $30 billion in 2020, with significant growth of electric vehicles and energy storage systems. Hence, cost-effective post-LIBs, such as SIBs and Mg batteries, could become more competitive in future markets. The monovalency of the carrier ions is another advantage, because a large portion of the knowledge that has been accumulated during the research of LIBs can be translated to SIBs. However, the larger size of the Na ion leads to considerable differences in the favoured crystal structure and intercalation behaviour. For the same host structure, the electrochemical performance of SIBs is usually inferior to that of LIBs, which imposes a hurdle for SIBs to be a competitive practical option[166]. A recent cost analysis highlighted this problem[167]; that is, the lower cost of the Na precursor materials is not sufficient to compensate for the inferior energy densities of SIBs. Although Na precursors (for example, Na_2CO_3) are about 25–30 times cheaper than Li precursors (for example, Li_2CO_3), the cost of the carrier ion accounts for a only a small fraction of the overall material cost, and a greater cost reduction may be provided by the use of Al as the anode current collector[167]. Thus, both the energy densities and cost per Watt-hour of SIBs need to be improved in parallel for them to become competitive on the global battery market.

For the cathode, in contrast to LIBs in which layered materials have been adopted for most applications, SIB research remains at the stage of identifying suitable materials. Over the past decade, both layered and polyanionic structures have been considered[166]. Na-ion (de) intercalation with layered materials was first reported by Delmas *et al.*[168] in the 1980s. In general, layered materials exhibit larger specific capacities but are less stable in long-term cycling owing to their structural instability upon Na-ion extraction. In layered structures, in contrast to LIBs in which Li ions are stored in the octahedral sites of an 'octahedral (O)-type' framework, the diffusion of Na ions is more stable when stored in the more spacious prismatic sites of a 'prismatic (P)-type' framework[169]. Moreover, most P-type structures are synthesized in Na-deficient forms with a Na stoichiometric fraction of about 0.7, which is detrimental to the full-cell energy density. Most layered SIB cathode materials exhibit operating voltages of up to 1.5 V lower than those of their layered LIB counterparts[170], which is the main factor responsible for the lower energy densities of SIBs. Nevertheless, an exceptional case was recently reported for O3-type $NaCrO_2$, which exhibits a rate and cycling performance[171] comparable to that of LIB materials with the same structure; thus, further exploration of layered materials is justified. In addition, it was demonstrated that the kinetics of $NaNi_{0.5}Mn_{0.5}O_2$ cathodes are superior to those of the lithium counterpart ($LiNi_{0.5}Mn_{0.5}O_2$), although the stability of $NaNi_{0.5}Mn_{0.5}O_2$ during prolonged cycling is uncertain[172]. By contrast, several polyanionic structures show stable long-term cycling performance, indicative of robust phase transitions during repeated charge–discharge cycles. Although the heavy anions of the polyanionic hosts are compensated for by multiple Na ions, the specific capacities are lower than those of their layered counterparts. At present, both categories of materials are in competition and represent a trade-off between specific capacity and cyclability. The voltages and capacities of representative SIB cathodes are summarized in FIG. 7a.

Progress in the development of the anode is even slower. Graphite, the most widely used anode material in LIBs, is inactive towards Na ions. Currently, hard carbon with ~300 mAh g^{-1} in the range of 1.2–0.1 V versus Na/Na^+ is the most commonly used material and serves as a reference for the study of other materials[166]. Na-ion diffusion in hard carbon occurs along channels and cavities with an irregular geometry, causing relatively poor rate performance. $NaTi_2(PO_4)_3$ (2.15 V, 132 mAh g^{-1})[173], $Na_2Ti_3O_7$ (0.3 V, 200 mAh g^{-1})[174], $Na_2Ti_6O_{13}$ (0.8 V, 65 mAh g^{-1})[175] and $NaTiO_2$ (1.1 V, 152 mAh g^{-1})[176], which all engage $Ti^{3+/4+}$ as redox centres, are another intercalation-based group of materials, but their specific capacities are relatively small. The material pool has been expanded to include those that can store Na ions on the basis of alloying and conversion mechanisms[177]. Sn (REFS 178,179), P (REFS 180–182), Sb (REFS 183–185), Ge (REFS 186,187), In (REF. 188) and their alloys[189–191], together with oxides[192–194], sulfides[195,196] and phosphides[197,198], are good examples. Similar to LIB materials operating via the same mechanisms (that is, alloying and conversion), the main issue with these materials is the limited long-term cyclability of the electrodes owing to the volume expansion of the active phases and the resultant unstable interfaces[199]. Some organic materials[200,201] with reasonably low operating voltages have also been introduced as SIB anodes, but their feasibility under practical conditions is yet to be verified. Although it is probable that only small molecules are competitive against other non-organic counterparts in terms of the specific capacity, factors such as their solubility in

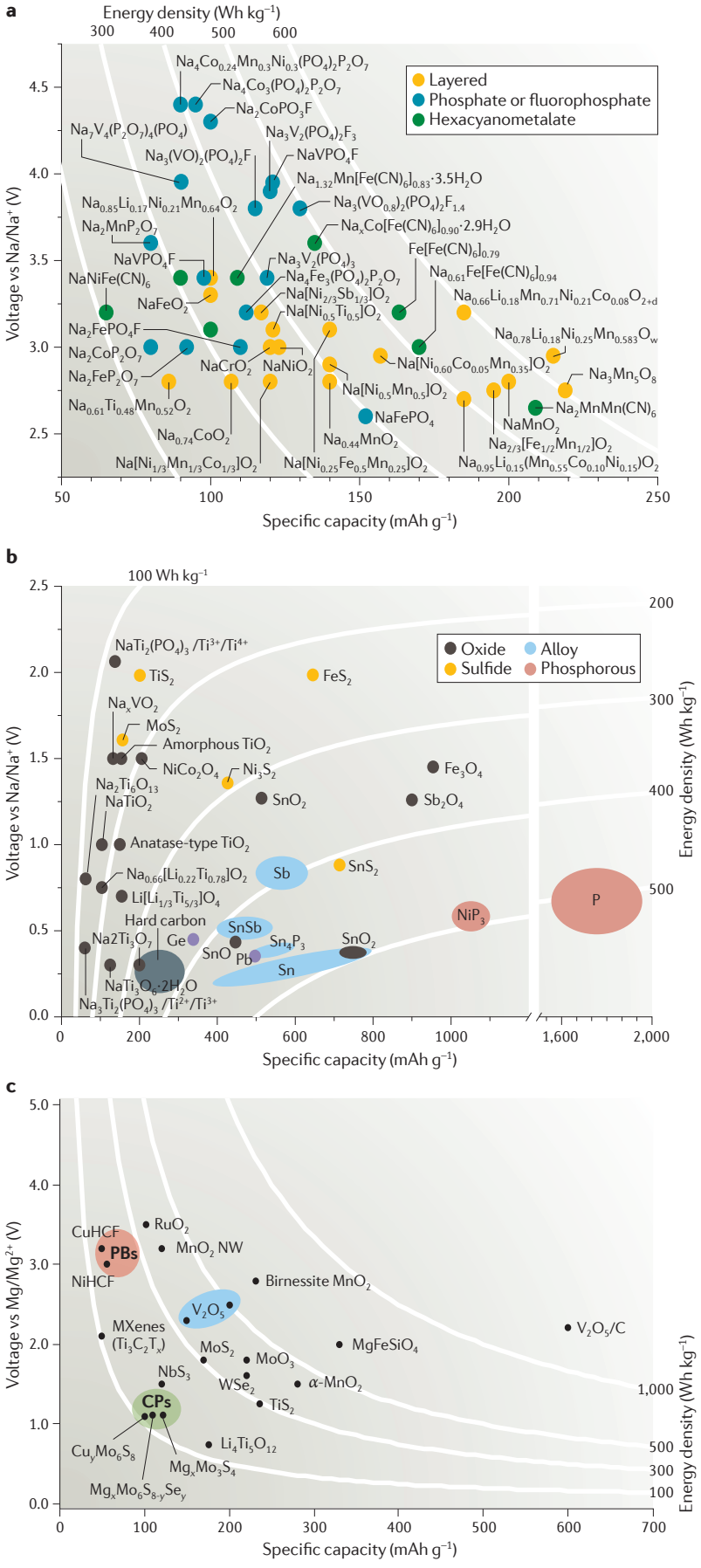

electrolytes at various potentials and poor adhesion to the current collector might create a nontrivial hurdle to overcome. The voltages and capacities of representative SIB anodes are summarized in FIG. 7b.

It has been reported[166] that the energy densities of some pairs of intercalation cathode materials and hard carbons in SIBs could be as high as that of a manganese spinel–graphite pair in LIBs. However, it should be noted that the energy density of LIBs consisting of mostly layered cathode–graphite pairs is still considerably higher. Hence, SIBs may be competitive with LIBs in certain applications in which cost is an important factor: that is, when a lower cost per unit energy density of SIBs can be reached. To evaluate the energy density, we chose $NaNi_{0.6}Co_{0.05}Mn_{0.35}O_2$ (REF. 202) as the cathode and hard carbon as the anode (Supplementary information S14 (table)). We excluded other Na-deficient phases, even those with higher specific capacities, because it is unclear how Na deficiency can be compensated. Under the same pouch-cell conditions used to evaluate the other battery systems in this Review (FIG. 1c), the $NaNi_{0.6}Co_{0.05}Mn_{0.35}O_2$–hard carbon cell offers a volumetric energy density of 267 Wh l^{-1}, which is only ~54% of that of $LiCoO_2$–graphite LIBs. One of the main reasons for the inferior energy density is the lower electrode densities of both electrodes compared with those of the LIBs, which results in a decrease in the number of stacks. If it is assumed that an anode with the same properties as graphite in LIBs can be developed, the energy density is expected to rise by ~45% to 388 Wh l^{-1} (Supplementary information S15 (table)), signifying the importance of finding high-capacity anode materials with high densities.

As SIBs mostly target large-scale energy storage systems, an energy-normalized cost analysis would be useful in assessing the value of each SIB. By taking the material prices available as of September 2015, we estimated the cost required for the pouch cell in FIG. 1c for both representative LIB and SIB cells (Supplementary information S16 (table) and Supplementary information S17 (table)). These values are normalized by the total energies in Supplementary information S2,S14 (tables), resulting in the energy-normalized cost of $0.11 and $0.14 per Wh (Supplementary information S16,17 (tables)) for the LIB and SIB cells, respectively. These values imply that even if the raw materials of SIBs are cheaper, the energy densities of SIBs need to be improved considerably to compete with LIBs in cost-sensitive, large-scale applications.

Rechargeable magnesium batteries. Mg batteries can store two electrons per Mg ion, which is beneficial for achieving high volumetric energy density[203,204]. Mg batteries combine the advantages of having a high theoretical volumetric capacity of the Mg-metal anode (3,833 versus 2,046 mAh cm^{-3} for a Li-metal anode), an

Figure 7 | **Operation voltages versus specific capacities of sodium-ion battery and magnesium battery electrode materials. a** | Sodium-ion battery (SIB) cathode materials. **b** | SIB anode materials. **c** | Mg battery cathode materials. CPs, Chevrel phases; HCF, hexacyanoferrate; PBs, Prussian blue.

abundance and low cost of Mg, and superior safety[203,204]. Nevertheless, since the first demonstration of reversible operation[205] by the Gregory group in 1990 and our demonstration of more practical prototype cells[206] in 2000, the technology is still at the basic research stage and the electrochemical performance of most reported cells is far inferior to that of LIBs and even to that of SIB prototypes. With regard to the electrolyte, several families of electrolyte solutions have recently been identified that enable a fully reversible reaction in Mg anodes with an anodic stability of >3 V versus the Mg anode[204,207,208]. In the cathodes, the greater electrostatic interaction between Mg^{2+} and host anions, compared with monovalent cations such as Na^+ and Li^+, slows the rate of Mg^{2+} diffusion, which impairs the overall electrochemical performance[203,204]. Interestingly, the performance of some materials was misinterpreted because of side reactions of the current collectors[209]. Starting with the Chevrel phases ($Mg_xMo_6S_{8-n}Se_n$, $n = 1$ or 2; $0 < x < 2$)[203,206], the materials pool has been expanded to include various oxides[210–212], chalcogenides[213,214], silicates[215], 2D early transition-metal carbides and carbonitrides — MXenes, ($M_{n+1}AX_n$: M = transition metal; A=Al, Ga, Si or Ge; X = C or N)[216,217] — and the Prussian blue family[218,219]. The operating voltages as a function of specific capacity of representative materials are summarized in FIG. 7c.

With respect to the electrolyte, since the initial Grignard solution[220] (RMgX in ethers, R = organic alkyl or aryl groups, X = Cl or Br) in the 1920s, successful research efforts have involved finding new compositions that allow reversible Mg deposition and dissolution on the Mg-anode surface and that simultaneously widen the stable voltage window. Mg organoborate moieties, such as $Mg(BBu_2Ph_2)_2$ in THF, were the first non-Grignard electrolytes used[205]. This is considered as the first major breakthrough in electrolyte research for Mg batteries, although the stable voltage range of such organometallic electrolytes is only up to ~1.9 V versus Mg/Mg^{2+}. The second breakthrough in this area was the use of the magnesium halo-alkyl aluminate complex ($Mg(AlCl_2BuEt)_2$) as the electrolyte[206] in the first prototype cell with a stable voltage range of up to ~2.2 V. The stable potential window of organometallic salts continues to be increased: for example, all-phenyl complexes[203] $(R_2Mg)_n(AlCl_{3-n}R'_n)_m$ (PhMgCl and $AlCl_3$), Grignard hexamethyldisilazane magnesium chloride (HMDS–MgCl)[221], and tri(3,5-dimethylphenyl)borane (Mes_3B) and PhMgCl in THF[222] have been reported to operate with a stable voltage of up to 3, 3.5 and 3.5 V, respectively. In the area of non-organometallic electrolytes, the community has tried to adopt less-volatile solvents, such as dimethylether (DME) and tetraglyme, and the magnesium aluminium chloride complex, $MgCl_2$–$AlCl_3$, in DME is the first good example in this direction[208]. Recently, $MgTFSI_2$–$MgCl_2$ in DME was also found to be promising[223]. Despite the good performance achieved with these organometallic and non-organometallic electrolytes, the corrosion of aluminium and stainless steel current collectors owing to the presence of halide ions hinders their practical use. Hence, electrolytes based on halide-free salts have recently been pursued[224–226]. Remarkably, Mohtadi *et al.* reported Mg batteries with boron-based, halide-free electrolytes, such as $Mg(BH_4)_2$ in DME[224] and $MgB_{12}H_{12}$ in THF[225]. This group subsequently reported[226] $Mg(CB_{11}H_{12})_2$ in tetraglyme with good solubility and high voltage stability of up to 3.8 V, and this discovery is worthy of being considered as the third breakthrough in the area of Mg-battery electrolytes.

We also evaluated the energy densities of Mg batteries (Supplementary information S18 (table)) when the Chevrel phase Mo_3S_4 with 122 mAh g^{-1} is used as a cathode at an operating cell voltage of 1.1 V. The most critical parameter in this estimation is the excess amount of Mg metal. With 50% excess, the given stacked cell has an energy density of 790 Wh l^{-1} — about 1.6 times as high as that of graphite–$LiCoO_2$ LIBs — justifying the continued research on the cathodes and electrolyte solutions for Mg batteries. When the excess amount of Mg metal changed to 0% and 100%, the energy density changed to 905 and 695 Wh l^{-1}, respectively.

Conclusions and outlook

The present IT and transportation technologies are more dependent on rechargeable batteries than at any time before, with a strong demand for enhanced energy density. In this Review, we have addressed materials and systems that are considered to be the most promising in this direction. However, when critically evaluated under a realistic battery platform, it appears that, in certain systems, the performance has been overestimated on the basis of the gravimetric capacities of the active materials, clarifying the importance of a balanced view of the materials and cells. In practice, the high theoretical gram-based capacities of active materials in most post-LIBs are not fully translated into volume-based cell energy densities, because a good portion of the capacity is lost owing to the low electrode densities and dead volume of the cell accessories. Hence, careful electrode optimization and cell design are essential for post-LIBs to take advantage of their material superiority and eventually fulfil their mission of surpassing state-of-the-art LIBs. In addition, once the lifetime of each post-LIB can be accurately specified, its end-of-life energy density can be evaluated, which, in turn, will allow the excess energy required in the initial cell (the 'overdesign') to be estimated.

Back to fundamentals with fresh ideas. In addition to the energy density, the issues related to the stable, long-term operation of post-LIBs need to be fundamentally resolved. Ironically, even when emerging advanced batteries malfunction, the problems begin from the same origins as in many historic batteries: irreversible phase transitions of active materials and/or unstable electrode/electrolyte solution interfaces. These common features reconfirm that for the successful development of post-LIBs and for possible commercialization, the stability of the electrodes and their interfaces over repeated charge–discharge cycles must be the focus of future research efforts. Considering the level of difficulty experienced to date, the existing problems of post-LIBs may need to be re-approached with fresh and creative remedies beyond the boundaries explored so far.

1. Tarascon, J. M. & Armand, M. Issues and challenges facing rechargeable lithium batteries. *Nature* **414**, 359–367 (2001).
2. Etacheri, V., Marom, R., Elazari, R., Salitra, G. & Aurbach, D. Challenges in the development of advanced Li-ion batteries: a review. *Energy Environ. Sci.* **4**, 3243–3262 (2011).
3. International Energy Agency. *Global EV outlook. Understanding the electric vehicle landscape to 2020* (IEA, 2013).
4. Armand, M. & Tarascon, J. M. Building better batteries. *Nature* **451**, 652–657 (2008).
5. Bruce, P. G., Freunberger, S. A., Hardwick, L. J. & Tarascon, J.-M. Li–O_2 and Li–S batteries with high energy storage. *Nat. Mater.* **11**, 19–29 (2012).
The operating principles, advantages and remaining issues of Li–S and Li–O_2 batteries are comprehensively reviewed in this article.
6. Cabana, J., Monconduit, L., Larcher, D. & Palacín, M. R. Beyond intercalation-based Li-ion batteries: the state of the art and challenges of electrode materials reacting through conversion reactions. *Adv. Mater.* **22**, E170–E192 (2010).
7. Dunn, B., Kamath, H. & Tarascon, J.-M. Electrical energy storage for the grid: a battery of choices. *Science* **334**, 928–935 (2011).
8. Goodenough, J. B. & Kim, Y. Challenges for rechargeable Li batteries. *Chem. Mater.* **22**, 587–603 (2010).
9. Thackeray, M. M., Wolverton, C. & Isaacs, E. D. Electrical energy storage for transportation—approaching the limits of, and going beyond, lithium-ion batteries. *Energy Environ. Sci.* **5**, 7854–7863 (2012).
10. Duduta, M. *et al.* Semi-solid lithium rechargeable flow battery. *Adv. Energy Mater.* **1**, 511–516 (2011).
11. Howard, W. F. & Spotnitz, R. M. Theoretical evaluation of high-energy lithium metal phosphate cathode materials in Li-ion batteries. *J. Power Sources* **165**, 887–891 (2007).
12. Yazami, R. & Touzain, P. A reversible graphite–lithium negative electrode for electrochemical generators. *J. Power Sources* **9**, 365–371 (1983).
13. Winter, M., Besenhard, J. O., Spahr, M. E. & Novák, P. Insertion electrode materials for rechargeable lithium batteries. *Adv. Mater.* **10**, 725–763 (1998).
14. Huggins, R. A. Lithium alloy negative electrodes. *J. Power Sources* **81–82**, 13–19 (1999).
15. Beaulieu, L. Y., Eberman, K. W., Turner, R. L., Krause, L. J. & Dahn, J. R. Colossal reversible volume changes in lithium alloys. *Electrochem. Solid State Lett.* **4**, A137–A140 (2001).
16. Wu, H. & Cui, Y. Designing nanostructured Si anodes for high energy lithium ion batteries. *Nano Today* **7**, 414–429 (2012).
In this article, issues originating from the volume expansion of Si active materials and the solutions based on nanostructural designs are discussed.
17. McDowell, M. T., Lee, S. W., Nix, W. D. & Cui, Y. 25th anniversary article: understanding the lithiation of silicon and other alloying anodes for lithium-ion batteries. *Adv. Mater.* **25**, 4966–4985 (2013).
18. Nelson, P. A. *et al.* High-performance batteries for off-peak energy storage and electric-vehicle propulsion, progress report. (Argonne National Laboratory, 1976).
19. Sharma, R. A. & Seefurth, R. N. Thermodynamic properties of the lithium–silicon system. *J. Electrochem. Soc.* **123**, 1763–1768 (1976).
20. Seefurth, R. N. & Sharma, R. A. Investigation of lithium utilization from a lithium–silicon electrode. *J. Electrochem. Soc.* **124**, 1207–1214 (1977).
21. Wilson, A. M. & Dahn, J. R. Lithium insertion in carbons containing nanodispersed silicon. *J. Electrochem. Soc.* **142**, 326–332 (1995).
22. Yu, Y. *et al.* Reversible storage of lithium in silver-coated three-dimensional macroporous silicon. *Adv. Mater.* **22**, 2247–2250 (2010).
23. Hwang, T. H., Lee, Y. M., Kong, B.-S., Seo, J.-S. & Choi, J. W. Electrospun core–shell fibers for robust silicon nanoparticle-based lithium ion battery anodes. *Nano Lett.* **12**, 802–807 (2012).
24. Liu, N. *et al.* A yolk-shell design for stabilized and scalable Li-ion battery alloy anodes. *Nano Lett.* **12**, 3315–3321 (2012).
25. Jung, D. S., Hwang, T. H., Park, S. B. & Choi, J. W. Spray drying method for large-scale and high-performance silicon negative electrodes in Li-ion batteries. *Nano Lett.* **13**, 2092–2097 (2013).
26. Son, I. H. *et al.* Silicon carbide-free graphene growth on silicon for lithium-ion battery with high volumetric energy density. *Nat. Commun.* **6**, 7393 (2015).
27. Koo, B. *et al.* A highly cross-linked polymeric binder for high-performance silicon negative electrodes in lithium ion batteries. *Angew. Chem. Int. Ed. Engl.* **51**, 8762–8767 (2012).
28. Kwon, T.-w. *et al.* Systematic molecular-level design of binders incorporating meldrum's acid for silicon anodes in lithium rechargeable batteries. *Adv. Mater.* **26**, 7979–7985 (2014).
29. Wang, C. *et al.* Self-healing chemistry enables the stable operation of silicon microparticle anodes for high-energy lithium-ion batteries. *Nat. Chem.* **5**, 1042–1048 (2013).
30. Chen, Z. *et al.* High-areal-capacity silicon electrodes with low-cost silicon particles based on spatial control of self-healing binder. *Adv. Energy Mater.* **5**, 1401826 (2015).
31. Li, J., Lewis, R. B. & Dahn, J. R. Sodium carboxymethyl cellulose: a potential binder for Si negative electrodes for Li-ion batteries. *Electrochem. Solid State Lett.* **10**, A17–A20 (2007).
32. Kovalenko, I. *et al.* A major constituent of brown algae for use in high-capacity Li-ion batteries. *Science* **334**, 75–79 (2011).
33. Murase, M. *et al.* Crop-derived polysaccharides as binders for high-capacity silicon/graphite-based electrodes in lithium-ion batteries. *ChemSusChem* **5**, 2307–2311 (2012).
34. Jeong, Y. K. *et al.* Hyperbranched β-cyclodextrin polymer as an effective multidimensional binder for silicon anodes in lithium rechargeable batteries. *Nano Lett.* **14**, 864–870 (2014).
35. Jeong, Y. K. *et al.* Millipede-inspired structural design principle for high performance polysaccharide binders in silicon anodes. *Energy Environ. Sci.* **8**, 1224–1230 (2015).
36. Liu, G. *et al.* Polymers with tailored electronic structure for high capacity lithium battery electrodes. *Adv. Mater.* **23**, 4679–4683 (2011).
37. Wu, H. *et al.* Stable Li-ion battery anodes by *in situ* polymerization of conducting hydrogel to conformally coat silicon nanoparticles. *Nat. Commun.* **4**, 1943 (2013).
38. Erickson, E. M. *et al.* Review — development of advanced rechargeable batteries: a continuous challenge in the choice of suitable electrolyte solutions. *J. Electrochem. Soc.* **162**, A2424–A2438 (2015).
39. Etacheri, V. *et al.* Exceptional electrochemical performance of Si nanowires in 1,3-dioxolane solutions: a surface chemical investigation. *Langmuir* **28**, 6175–6184 (2012).
40. Markevich, E. *et al.* Amorphous columnar silicon anodes for advanced high voltage lithium ion full cells: dominant factors governing cycling performance. *J. Electrochem. Soc.* **160**, A1824–A1833 (2013).
41. Markevich, E. *et al.* High performance of thick amorphous columnar monolithic film silicon anodes in ionic liquid electrolytes at elevated temperature. *RSC Adv.* **4**, 48572–48575 (2014).
42. Fukuoka, H., Aramata, M. & Miyawaki, S. Method for producing SiO_x ($x < 1$). US Patent 0254102 (2007).
43. DeWet Erasmus, H. & Persson, J. A. Preparation and properties of silicon monoxide. *J. Electrochem. Soc.* **95**, 316–318 (1949).
44. Park, E. *et al.* Dual-size silicon nanocrystal-embedded SiO_x nanocomposite as a high-capacity lithium storage material. *ACS Nano* **9**, 7690–7696 (2015).
45. Doh, C.-H. *et al.* A new SiO/C anode composition for lithium-ion battery. *J. Power Sources* **179**, 367–370 (2008).
46. Zhao, J. *et al.* Dry-air-stable lithium silicide–lithium oxide core–shell nanoparticles as high-capacity prelithiation reagents. *Nat. Commun.* **5**, 5088 (2014).
47. Liu, N., Hu, L., McDowell, M. T., Jackson, A. & Cui, Y. Prelithiated silicon nanowires as an anode for lithium ion batteries. *ACS Nano* **5**, 6487–6493 (2011).
48. Kim, H. J. *et al.* Controlled prelithiation of silicon monoxide for high performance lithium-ion rechargeable full cells. *Nano Lett.* **16**, 282–288 (2015).
49. Miyachi, M., Yamamoto, H., Kawai, H., Ohta, T. & Shirakata, M. Analysis of SiO anodes for lithium-ion batteries. *J. Electrochem. Soc.* **152**, A2089–A2091 (2005).
50. Komaba, S. *et al.* Study on polymer binders for high-capacity SiO negative electrode of Li-ion batteries. *J. Phys. Chem. C* **115**, 13487–13495 (2011).
51. Rossen, E., Jones, C. D. W. & Dahn, J. R. Structure and electrochemistry of $Li_xMn_yNi_{1-y}O_2$. *Solid State Ionics* **57**, 311–318 (1992).
52. Rossouw, M. H., Liles, D. C. & Thackeray, M. M. Synthesis and structural characterization of a novel layered lithium manganese oxide, $Li_{0.36}Mn_{0.91}O_2$, and its lithiated derivative, $Li_{1.09}Mn_{0.91}O_2$. *J. Solid State Chem.* **104**, 464–466 (1993).
53. Chikkannanavar, S. B., Bernardi, D. M. & Liu, L. A review of blended cathode materials for use in Li-ion batteries. *J. Power Sources* **248**, 91–100 (2014).
54. Jung, S.-K. *et al.* Understanding the degradation mechanisms of $LiNi_{0.5}Co_{0.2}Mn_{0.3}O_2$ cathode material in lithium ion batteries. *Adv. Energy Mater.* **4**, 1300787 (2014).
55. Chen, C. H. *et al.* Aluminum-doped lithium nickel cobalt oxide electrodes for high-power lithium-ion batteries. *J. Power Sources* **128**, 278–285 (2004).
56. Manthiram, A., Knight, J. C., Myung, S.-T., Oh, S.-M. & Sun, Y.-K. Nickel-rich and lithium-rich layered oxide cathodes: progress and perspectives. *Adv. Energy Mater.* **6**, 1501010 (2015).
This article addresses key challenges in the synthesis and battery operation of high-capacity layered oxide cathodes and outlines future research directions.
57. Liu, W. *et al.* Nickel-rich layered lithium transition-metal oxide for high-energy lithium-ion batteries. *Angew. Chem. Int. Ed. Engl.* **54**, 4440–4457 (2015).
58. Lin, F. *et al.* Surface reconstruction and chemical evolution of stoichiometric layered cathode materials for lithium-ion batteries. *Nat. Commun.* **5**, 3529 (2014).
59. Johnson, C. S., Li, N., Lefief, C., Vaughey, J. T. & Thackeray, M. M. Synthesis, characterization and electrochemistry of lithium battery electrodes: $xLi_2MnO_3{\cdot}(1-x)LiMn_{0.333}Ni_{0.333}Co_{0.333}O_2$ ($0 \le x \le 0.7$). *Chem. Mater.* **20**, 6095–6106 (2008).
60. Lee, K.-S., Myung, S.-T., Amine, K., Yashiro, H. & Sun, Y.-K. Structural and electrochemical properties of layered $Li[Ni_{1-2x}Co_xMn_x]O_2$ (x = 0.1–0.3) positive electrode materials for Li-ion batteries. *J. Electrochem. Soc.* **154**, A971–A977 (2007).
61. Nayak, P. K., Grinblat, J., Levi, M., Markovsky, B. & Aurbach, D. Structural and electrochemical evidence of layered to spinel phase transformation of Li and Mn rich layered cathode materials of the formulae $xLi[Li_{1/3}Mn_{2/3}]O_2{\cdot}(1-x)LiMn_{1/3}Ni_{1/3}Co_{1/3}O_2$ (x = 0.2, 0.4, 0.6) upon cycling. *J. Electrochem. Soc.* **161**, A1534–A1547 (2014).
62. Haik, O. *et al.* On the surface chemistry of $LiMO_2$ cathode materials (M = [MnNi] and [MnNiCo]): electrochemical, spectroscopic, and calorimetric studies. *J. Electrochem. Soc.* **157**, A1099–A1107 (2010).
63. Kam, K. C., Mehta, A., Heron, J. T. & Doeff, M. M. Electrochemical and physical properties of Ti-substituted layered nickel manganese cobalt oxide (NMC) cathode materials. *J. Electrochem. Soc.* **159**, A1383–A1392 (2012).
64. Karan, N. *et al.* Structural characteristics and electrochemical performance of layered $Li[Mn_{0.5-x}Cr_{2x}Ni_{0.5-x}]O_2$ cathode materials. *J. Power Sources* **187**, 586–590 (2009).
65. Kim, J. & Amine, K. A comparative study on the substitution of divalent, trivalent and tetravalent metal ions in $LiNi_{1-x}M_xO_2$ ($M = Cu^{2+}$, Al^{3+} and Ti^{4+}). *J. Power Sources* **104**, 33–39 (2002).
66. Kim, H.-B. *et al.* Electrochemical and thermal characterization of AlF_3-coated $Li[Ni_{0.8}Co_{0.15}Al_{0.05}]O_2$ cathode in lithium-ion cells. *J. Power Sources* **179**, 347–350 (2008).
67. West, W. *et al.* Electrochemical behavior of layered solid solution Li_2MnO_3 – $LiMO_2$ (M = Ni, Mn, Co) Li-ion cathodes with and without alumina coatings. *J. Electrochem. Soc.* **158**, A883–A889 (2011).
68. Zhang, X. *et al.* Structural and electrochemical study of Al_2O_3 and TiO_2 coated $Li_{1.2}Ni_{0.13}Mn_{0.54}Co_{0.13}O_2$ cathode material using ALD. *Adv. Energy Mater.* **3**, 1299–1307 (2013).
69. Cho, J., Kim, H. & Park, B. Comparison of overcharge behavior of $AlPO_4$-coated $LiCoO_2$ and $LiNi_{0.8}Co_{0.1}Mn_{0.1}O_2$ cathode materials in Li-ion cells. *J. Electrochem. Soc.* **151**, A1707–A1711 (2004).
70. Ma, X., Wang, C., Han, X. & Sun, J. Effect of $AlPO_4$ coating on the electrochemical properties of $LiNi_{0.8}Co_{0.2}O_2$ cathode material. *J. Alloys Compd.* **453**, 352–355 (2008).
71. Liu, J., Wang, Q., Reeja-Jayan, B. & Manthiram, A. Carbon-coated high capacity layered $Li[Li_{0.2}Mn_{0.54}Ni_{0.13}Co_{0.13}]O_2$ cathodes. *Electrochem. Commun.* **12**, 750–753 (2010).
72. Chen, Y., Zhang, Y., Chen, B., Wang, Z. & Lu, C. An approach to application for $LiNi_{0.6}Co_{0.2}Mn_{0.2}O_2$ cathode material at high cutoff voltage by TiO_2 coating. *J. Power Sources* **256**, 20–27 (2014).

73. Zheng, J., Li, J., Zhang, Z., Guo, X. & Yang, Y. The effects of TiO_2 coating on the electrochemical performance of $Li[Li_{0.2}Mn_{0.54}Ni_{0.13}Co_{0.13}]O_2$ cathode material for lithium-ion battery. *Solid State Ionics* **179**, 1794–1799 (2008).
74. Cho, Y., Lee, S., Lee, Y., Hong, T. & Cho, J. Spinel-layered core–shell cathode materials for Li-ion batteries. *Adv. Energy Mater.* **1**, 821–828 (2011).
75. Wu, F. *et al.* Ultrathin spinel membrane-encapsulated layered lithium-rich cathode material for advanced Li-ion batteries. *Nano Lett.* **14**, 3550–3555 (2014).
76. Sun, Y.-K. *et al.* Nanostructured high-energy cathode materials for advanced lithium batteries. *Nat. Mater.* **11**, 942–947 (2012).
77. Whittingham, M. S. Electrical energy storage and intercalation chemistry. *Science* **192**, 1126–1127 (1976).
78. Aurbach, D., Zinigrad, E., Cohen, Y. & Teller, H. A short review of failure mechanisms of lithium metal and lithiated graphite anodes in liquid electrolyte solutions. *Solid State Ionics* **148**, 405–416 (2002).
79. Xu, W. *et al.* Lithium metal anodes for rechargeable batteries. *Energy Environ. Sci.* **7**, 513–537 (2014). **The factors that affect undesirable dendrite growth and poor Coulombic efficiency in Li-metal anodes are summarized in this article, along with recent developments to mitigate the problem.**
80. Aurbach, D., Zinigrad, E., Teller, H. & Dan, P. Factors which limit the cycle life of rechargeable lithium (metal) batteries. *J. Electrochem. Soc.* **147**, 1274–1279 (2000).
81. Yu, X., Bates, J. B., Jellison, G. E. & Hart, F. X. A stable thin-film lithium electrolyte: lithium phosphorus oxynitride. *J. Electrochem. Soc.* **144**, 524–532 (1997).
82. Kozen, A. C. *et al.* Next-generation lithium metal anode engineering via atomic layer deposition. *ACS Nano* **9**, 5884–5892 (2015).
83. Lee, H., Lee, D. J., Kim, Y.-J., Park, J.-K. & Kim, H.-T. A simple composite protective layer coating that enhances the cycling stability of lithium metal batteries. *J. Power Sources* **284**, 103–108 (2015).
84. Zheng, G. *et al.* Interconnected hollow carbon nanospheres for stable lithium metal anodes. *Nat. Nanotechnol.* **9**, 618–623 (2014).
85. Kim, J.-S., Kim, D. W., Jung, H. T. & Choi, J. W. Controlled lithium dendrite growth by a synergistic effect of multilayered graphene coating and an electrolyte additive. *Chem. Mater.* **27**, 2780–2787 (2015).
86. Ryou, M.-H. *et al.* Excellent cycle life of lithium-metal anodes in lithium-ion batteries with mussel-inspired polydopamine-coated separators. *Adv. Energy Mater.* **2**, 645–650 (2012).
87. Lu, Y., Tu, Z. & Archer, L. A. Stable lithium electrodeposition in liquid and nanoporous solid electrolytes. *Nat. Mater.* **13**, 961–969 (2014).
88. Aurbach, D. *et al.* Design of electrolyte solutions for Li and Li-ion batteries: a review. *Electrochim. Acta* **50**, 247–254 (2004).
89. Ota, H., Shima, K., Ue, M. & Yamaki, J.-i. Effect of vinylene carbonate as additive to electrolyte for lithium metal anode. *Electrochim. Acta* **49**, 565–572 (2004).
90. Lee, Y. M. *et al.* Effects of triacetoxyvinylsilane as SEI layer additive on electrochemical performance of lithium metal secondary battery. *Electrochem. Solid State Lett.* **10**, A216–A219 (2007).
91. Ding, F. *et al.* Dendrite-free lithium deposition via self-healing electrostatic shield mechanism. *J. Am. Chem. Soc.* **135**, 4450–4456 (2013).
92. Ryou, M.-H., Lee, Y. M., Lee, Y., Winter, M. & Bieker, P. Mechanical surface modification of lithium metal: towards improved Li metal anode performance by directed Li plating. *Adv. Funct. Mater.* **25**, 834–841 (2015).
93. Lee, J. H. *et al.* Effect of lithium powder size on the performance of lithium-powder/lithium trivanadate secondary batteries shown via impedance analysis. *Electrochim. Acta* **131**, 202–206 (2014).
94. Rao, M. L. B. Organic electrolyte cells. US Patent 3413154 (1968).
95. Rauh, R. D., Abraham, K. M., Pearson, G. F., Surprenant, J. K. & Brummer, S. B. Lithium-dissolved sulfur battery with an organic electrolyte. *J. Electrochem. Soc.* **126**, 523–527 (1979).
96. Aurbach, D. *et al.* On the surface chemical aspects of very high energy density, rechargeable Li–sulfur batteries. *J. Electrochem. Soc.* **156**, A694–A702 (2009).
97. Elazari, R. *et al.* Morphological and structural studies of composite sulfur electrodes upon cycling by HRTEM, AFM and Raman spectroscopy. *J. Electrochem. Soc.* **157**, A1131–A1138 (2010).
98. Ji, X. & Nazar, L. F. Advances in Li–S batteries. *J. Mater. Chem.* **20**, 9821–9826 (2010).
99. Yin, Y.-X., Xin, S., Guo, Y.-G. & Wan, L.-J. Lithium–sulfur batteries: electrochemistry, materials, and prospects. *Angew. Chem. Int. Ed. Engl.* **52**, 13186–13200 (2013).
100. Ji, X., Lee, K. T. & Nazar, L. F. A highly ordered nanostructured carbon–sulphur cathode for lithium–sulphur batteries. *Nat. Mater.* **8**, 500–506 (2009).
101. Elazari, R., Salitra, G., Garsuch, A., Panchenko, A. & Aurbach, D. Sulfur-impregnated activated carbon fiber cloth as a binder-free cathode for rechargeable Li–S batteries. *Adv. Mater.* **23**, 5641–5644 (2011).
102. Evers, S., Yim, T. & Nazar, L. F. Understanding the nature of absorption/adsorption in nanoporous polysulfide sorbents for the Li–S battery. *J. Phys. Chem. C* **116**, 19653–19658 (2012).
103. Song, J. *et al.* Nitrogen-doped mesoporous carbon promoted chemical adsorption of sulfur and fabrication of high-areal-capacity sulfur cathode with exceptional cycling stability for lithium–sulfur batteries. *Adv. Funct. Mater.* **24**, 1243–1250 (2014).
104. Xin, S. *et al.* Smaller sulfur molecules promise better lithium–sulfur batteries. *J. Am. Chem. Soc.* **134**, 18510–18513 (2012).
105. Kim, J.-S., Hwang, T. H., Kim, B. G., Min, J. & Choi, J. W. A lithium–sulfur battery with a high areal energy density. *Adv. Funct. Mater.* **24**, 5359–5367 (2014).
106. Chung, W. J. *et al.* The use of elemental sulfur as an alternative feedstock for polymeric materials. *Nat. Chem.* **5**, 518–524 (2013).
107. Nagao, M., Hayashi, A. & Tatsumisago, M. Electrochemical performance of all-solid-state Li/S batteries with sulfur-based composite electrodes prepared by mechanical milling at high temperature. *Energy Technol.* **1**, 186–192 (2013).
108. Machida, N., Kobayashi, K., Nishikawa, Y. & Shigematsu, T. Electrochemical properties of sulfur as cathode materials in a solid-state lithium battery with inorganic solid electrolytes. *Solid State Ionics* **175**, 247–250 (2004).
109. Kinoshita, S., Okuda, K., Machida, N., Naito, M. & Sigematsu, T. All-solid-state lithium battery with sulfur/carbon composites as positive electrode materials. *Solid State Ionics* **256**, 97–102 (2014).
110. Kobayashi, T. *et al.* All solid-state battery with sulfur electrode and thio-LISICON electrolyte. *J. Power Sources* **182**, 621–625 (2008).
111. Unemoto, A. *et al.* Development of bulk-type all-solid-state lithium–sulfur battery using $LiBH_4$ electrolyte. *Appl. Phys. Lett.* **105**, 083901 (2014).
112. Marmorstein, D. *et al.* Electrochemical performance of lithium/sulfur cells with three different polymer electrolytes. *J. Power Sources* **89**, 219–226 (2000).
113. Ryu, H.-S., Ahn, H.-J., Kim, K.-W., Ahn, J.-H. & Lee, J.-Y. Discharge process of Li/PVdF/S cells at room temperature. *J. Power Sources* **153**, 360–364 (2006).
114. Choi, J. W. *et al.* Microporous poly(vinylidene fluoride-*co*-hexafluoropropylene) polymer electrolytes for lithium/sulfur cells. *J. Ind. Eng. Chem.* **12**, 939–949 (2006).
115. Rao, M., Geng, X., Li, X., Hu, S. & Li, W. Lithium–sulfur cell with combining carbon nanofibers–sulfur cathode and gel polymer electrolyte. *J. Power Sources* **212**, 179–185 (2012).
116. Koh, J. Y. *et al.* Electrochemical reduction mechanism of sulfur particles electrically isolated from carbon cathodes of lithium–sulfur cells. *J. Electrochem. Soc.* **161**, A2117–A2120 (2014).
117. Markevich, E. *et al.* The effect of a solid electrolyte interphase on the mechanism of operation of lithium–sulfur batteries. *J. Mater. Chem. A* **3**, 19873–19883 (2015).
118. Markevich, E. *et al.* Fluoroethylene carbonate as an important component in organic carbonate electrolyte solutions for lithium sulfur batteries. *Electrochem. Commun.* **60**, 42–46 (2015).
119. Yuan, Z. *et al.* Hierarchical free-standing carbon-nanotube paper electrodes with ultrahigh sulfur-loading for lithium–sulfur batteries. *Adv. Funct. Mater.* **24**, 6105–6112 (2014).
120. Abraham, K. M. & Jiang, Z. A polymer electrolyte-based rechargeable lithium/oxygen battery. *J. Electrochem. Soc.* **143**, 1–5 (1996).
121. Li, Y. & Dai, H. Recent advances in zinc–air batteries. *Chem. Soc. Rev.* **43**, 5257–5275 (2014). **Detailed effects of cell components in primary and secondary Zn–air batteries on the electrochemical performance are discussed in this article, focusing on the cells' operation principles, technical issues and potential solutions.**
122. Palmer, N. J. Secondary metal/air cell. US Patent 3650837 (1972).
123. Shao, Y. *et al.* Making Li–air batteries rechargeable: material challenges. *Adv. Funct. Mater.* **23**, 987–1004 (2013).
124. Hasegawa, S. *et al.* Study on lithium/air secondary batteries — stability of NASICON-type lithium ion conducting glass–ceramics with water. *J. Power Sources* **189**, 371–377 (2009).
125. Visco, S. *et al.* Aqueous and nonaqueous lithium–air batteries enabled by water-stable lithium metal electrodes. *J. Solid State Electrochem.* **18**, 1443–1456 (2014).
126. Zhang, T. *et al.* Li/polymer electrolyte/water stable lithium-conducting glass ceramics composite for lithium–air secondary batteries with an aqueous electrolyte. *J. Electrochem. Soc.* **155**, A965–A969 (2008).
127. Visco, S. J., Katz, B. D., Nimon, Y. S. & De Jonghe, L. C. Protected active metal electrode and battery cell structures with non-aqueous interlayer architecture. US Patent 7282295 (2007).
128. Kim, B. G. *et al.* Improved reversibility in lithium–oxygen battery: understanding elementary reactions and surface charge engineering of metal alloy catalyst. *Sci. Rep.* **4**, 4225 (2014).
129. Freunberger, S. A. *et al.* The lithium–oxygen battery with ether-based electrolytes. *Angew. Chem. Int. Ed. Engl.* **50**, 8609–8613 (2011).
130. Ottakam Thotiyl, M. M., Freunberger, S. A., Peng, Z. & Bruce, P. G. The carbon electrode in nonaqueous Li–O_2 cells. *J. Am. Chem. Soc.* **135**, 494–500 (2013).
131. Kim, B. G., Kim, S., Lee, H. & Choi, J. W. Wisdom from the human eye: a synthetic melanin radical scavenger for improved cycle life of Li–O_2 battery. *Chem. Mater.* **26**, 4757–4764 (2014).
132. Peng, Z., Freunberger, S. A., Chen, Y. & Bruce, P. G. A reversible and higher-rate Li–O_2 battery. *Science* **337**, 563–566 (2012).
133. Harding, J. R., Lu, Y.-C., Tsukada, Y. & Shao-Horn, Y. Evidence of catalyzed oxidation of Li_2O_2 for rechargeable Li–air battery applications. *Phys. Chem. Chem. Phys.* **14**, 10540–10546 (2012).
134. Li, F. *et al.* Ru/ITO: a carbon-free cathode for nonaqueous Li–O_2 battery. *Nano Lett.* **13**, 4702–4707 (2013).
135. Lu, J. *et al.* A nanostructured cathode architecture for low charge overpotential in lithium–oxygen batteries. *Nat. Commun.* **4**, 2383 (2013).
136. Débart, A., Paterson, A. J., Bao, J. & Bruce, P. G. α-MnO_2 nanowires: a catalyst for the O_2 electrode in rechargeable lithium batteries. *Angew. Chem. Int. Ed. Engl.* **47**, 4521–4524 (2008).
137. Black, R., Lee, J.-H., Adams, B., Mims, C. A. & Nazar, L. F. The role of catalysts and peroxide oxidation in lithium–oxygen batteries. *Angew. Chem. Int. Ed. Engl.* **52**, 392–396 (2013).
138. Shang, C. *et al.* Compatible interface design of CoO-based Li–O_2 battery cathodes with long-cycling stability. *Sci. Rep.* **5**, 8335 (2015).
139. McCloskey, B. D. *et al.* On the efficacy of electrocatalysis in nonaqueous Li–O_2 batteries. *J. Am. Chem. Soc.* **133**, 18038–18041 (2011).
140. Grande, L. *et al.* The lithium/air battery: still an emerging system or a practical reality? *Adv. Mater.* **27**, 784–800 (2015).
141. Adams, B. D. *et al.* Current density dependence of peroxide formation in the Li–O_2 battery and its effect on charge. *Energy Environ. Sci.* **6**, 1772–1778 (2013).
142. Chen, Y., Freunberger, S. A., Peng, Z., Fontaine, O. & Bruce, P. G. Charging a Li–O_2 battery using a redox mediator. *Nat. Chem.* **5**, 489–494 (2013).
143. Lim, H.-D. *et al.* Superior rechargeability and efficiency of lithium–oxygen batteries: hierarchical air electrode architecture combined with a soluble catalyst. *Angew. Chem. Int. Ed. Engl.* **53**, 3926–3931 (2014).
144. Freunberger, S. A. *et al.* Reactions in the rechargeable lithium–O_2 battery with alkyl carbonate electrolytes. *J. Am. Chem. Soc.* **133**, 8040–8047 (2011).
145. Xu, D. Wang, Z.-l., Xu, J.-j., Zhang, L.-l. & Zhang, X.-b. Novel DMSO-based electrolyte for high performance rechargeable Li–O_2 batteries. *Chem. Commun.* **48**, 6948–6950 (2012).
146. Sharon, D. *et al.* On the challenge of electrolyte solutions for Li–air batteries: monitoring oxygen reduction and related reactions in polyether solutions by spectroscopy and EQCM. *J. Phys. Chem. Lett.* **4**, 127–131 (2013).
147. Sharon, D. *et al.* Oxidation of dimethyl sulfoxide solutions by electrochemical reduction of oxygen. *J. Phys. Chem. Lett.* **4**, 3115–3119 (2013).

148. Sharon, D. *et al.* Lithium–oxygen electrochemistry in non-aqueous solutions. *Isr. J. Chem.* **55**, 508–520 (2015).
149. Kwak, W.-J. *et al.* Understanding the behavior of Li–oxygen cells containing LiI. *J. Mater. Chem. A* **3**, 8855–8864 (2015).
150. Ottakam Thotiyl, M. M. *et al.* A stable cathode for the aprotic Li–O_2 battery. *Nat. Mater.* **12**, 1050–1056 (2013).
151. Kundu, D., Black, R., Berg, E. J. & Nazar, L. F. A highly active nanostructured metallic oxide cathode for aprotic Li–O_2 batteries. *Energy Environ. Sci.* **8**, 1292–1298 (2015).
152. Su, D., Dou, S. & Wang, G. Single crystalline Co_3O_4 nanocrystals exposed with different crystal planes for Li–O_2 batteries. *Sci. Rep.* **4**, 5767 (2014).
153. Kwak, W.-J. *et al.* A Mo_2C/carbon nanotube composite cathode for lithium–oxygen batteries with high energy efficiency and long cycle life. *ACS Nano* **9**, 4129–4137 (2015).
154. Li, F. *et al.* Superior performance of a Li–O_2 battery with metallic RuO_2 hollow spheres as the carbon-free cathode. *Adv. Energy Mater.* **5**, 1500294 (2015).
155. Kim, B. G., Lee, J.-N., Lee, D. J., Park, J.-K. & Choi, J. W. Robust cycling of Li–O_2 batteries through the synergistic effect of blended electrolytes. *ChemSusChem* **6**, 443–448 (2013).
156. Linden, D. & Reddy, T. B. *Handbook of Batteries* (McGraw-Hill, 2001).
157. Zhang, J., Zhao, Z., Xia, Z. & Dai, L. A metal-free bifunctional electrocatalyst for oxygen reduction and oxygen evolution reactions. *Nat. Nanotechnol.* **10**, 444–452 (2015).
158. Parker, J. F., Chervin, C. N., Nelson, E. S., Rolison, D. R. & Long, J. W. Wiring zinc in three dimensions re-writes battery performance-dendrite-free cycling. *Energy Environ. Sci.* **7**, 1117–1124 (2014).
159. Müller, S., Haas, O., Schlatter, C. & Comninellis, C. Development of a 100 W rechargeable bipolar zinc/oxygen battery. *J. Appl. Electrochem.* **28**, 305–310 (1998).
160. Vorkapič, L. Ž., Dražič, D. M. & Despič, A. R. Corrosion of pure and amalgamated zinc in concentrated alkali hydroxide solutions. *J. Electrochem. Soc.* **121**, 1385–1392 (1974).
161. Lee, C. W., Sathiyanarayanan, K., Eom, S. W. & Yun, M. S. Novel alloys to improve the electrochemical behavior of zinc anodes for zinc/air battery. *J. Power Sources* **160**, 1436–1441 (2006).
162. Ein-Eli, Y., Auinat, M. & Starosvetsky, D. Electrochemical and surface studies of zinc in alkaline solutions containing organic corrosion inhibitors. *J. Power Sources* **114**, 330–337 (2003).
163. Cho, Y.-D. & Fey, G. T.-K. Surface treatment of zinc anodes to improve discharge capacity and suppress hydrogen gas evolution. *J. Power Sources* **184**, 610–616 (2008).
164. Li, Y. *et al.* Advanced zinc–air batteries based on high-performance hybrid electrocatalysts. *Nat. Commun.* **4**, 1805 (2013).
165. Cheng, H.-H. & Tan, C.-S. Reduction of CO_2 concentration in a zinc/air battery by absorption in a rotating packed bed. *J. Power Sources* **162**, 1431–1436 (2006).
166. Yabuuchi, N., Kubota, K., Dahbi, M. & Komaba, S. Research development on sodium-ion batteries. *Chem. Rev.* **114**, 11636–11682 (2014).
This article details the motivation behind Na-ion batteries and provides a summary of the broad range of their positive and negative electrodes.
167. Kim, Y., Ha, K. H., Oh, S. M. & Lee, K. T. High-capacity anode materials for sodium-ion batteries. *Chem. Eur. J.* **20**, 11980–11992 (2014).
168. Delmas, C., Braconnier, J.-J., Fouassier, C. & Hagenmuller, P. Electrochemical intercalation of sodium in Na_xCoO_2 bronzes. *Solid State Ionics* **3–4**, 165–169 (1981).
169. Yabuuchi, N. *et al.* P2-type $Na_xFe_{1/2}Mn_{1/2}O_2$ made from earth-abundant elements for rechargeable Na batteries. *Nat. Mater.* **11**, 512–517 (2012).
170. Ong, S. P. *et al.* Voltage, stability and diffusion barrier differences between sodium-ion and lithium-ion intercalation materials. *Energy Environ. Sci.* **4**, 3680–3688 (2011).
171. Yu, C. Y. *et al.* $NaCrO_2$ cathode for high-rate sodium-ion batteries. *Energy Environ. Sci.* **8**, 2019–2026 (2015).
172. de la Llave, E. *et al.* Comparison between Na-ion and Li-ion cells: understanding the critical role of the cathodes stability and the anodes pretreatment on the cells behavior. *ACS Appl. Mater. Interfaces* **8**, 1867–1875 (2015).
173. Delmas, C., Cherkaoui, F., Nadiri, A. & Hagenmuller, P. A. NASICON-type phase as intercalation electrode: $NaTi_2(PO_4)_3$. *Mater. Res. Bull.* **22**, 631–639 (1987).
174. Senguttuvan, P., Rousse, G., Seznec, V., Tarascon, J.-M. & Rosa Palacin, M. $Na_2Ti_3O_7$: lowest voltage ever reported oxide insertion electrode for sodium ion batteries. *Chem. Mater.* **23**, 4109–4111 (2011).
175. Rudola, A., Saravanan, K., Devaraj, S., Gong, H. & Balaya, P. $Na_2Ti_6O_{13}$: a potential anode for grid-storage sodium-ion batteries. *Chem. Commun.* **49**, 7451–7453 (2013).
176. Wu, D. *et al.* $NaTiO_2$: a layered anode material for sodium-ion batteries. *Energy Environ. Sci.* **8**, 195–202 (2015).
177. Chevrier, V. L. & Ceder, G. Challenges for Na-ion negative electrodes. *J. Electrochem. Soc.* **158**, A1011–A1014 (2011).
178. Baggetto, L. *et al.* Characterization of sodium ion electrochemical reaction with tin anodes: experiment and theory. *J. Power Sources* **234**, 48–59 (2013).
179. Ellis, L. D., Hatchard, T. D. & Obrovac, M. N. Reversible insertion of sodium in tin. *J. Electrochem. Soc.* **159**, A1801–A1805 (2012).
180. Kim, Y. *et al.* An amorphous red phosphorus/carbon composite as a promising anode material for sodium ion batteries. *Adv. Mater.* **25**, 3045–3049 (2013).
181. Qian, J., Wu, X., Cao, Y., Ai, X. & Yang, H. High capacity and rate capability of amorphous phosphorus for sodium ion batteries. *Angew. Chem. Int. Ed. Engl.* **52**, 4633–4636 (2013).
182. Li, W.-J., Chou, S.-L., Wang, J.-Z., Liu, H.-K. & Dou, S.-X. Simply mixed commercial red phosphorus and carbon nanotube composite with exceptionally reversible sodium-ion storage. *Nano Lett.* **13**, 5480–5484 (2013).
183. Darwiche, A. *et al.* Better cycling performances of bulk Sb in Na-ion batteries compared to Li-ion systems: an unexpected electrochemical mechanism. *J. Am. Chem. Soc.* **135**, 10179–10179 (2013).
184. Baggetto, L. *et al.* Intrinsic thermodynamic and kinetic properties of Sb electrodes for Li-ion and Na-ion batteries: experiment and theory. *J. Mater. Chem. A* **1**, 7985–7994 (2013).
185. He, M., Kraychyk, K., Walter, M. & Kovalenko, M. V. Monodisperse antimony nanocrystals for high-rate Li-ion and Na-ion battery anodes: nano versus bulk. *Nano Lett.* **14**, 1255–1262 (2014).
186. Baggetto, L., Keum, J. K., Browning, J. F. & Veith, G. M. Germanium as negative electrode material for sodium-ion batteries. *Electrochem. Commun.* **34**, 41–44 (2013).
187. Abel, P. R. *et al.* Nanocolumnar germanium thin films as a high-rate sodium-ion battery anode material. *J. Phys. Chem. C* **117**, 18885–18890 (2013).
188. Webb, S. A., Baggetto, L., Bridges, C. A. & Veith, G. M. The electrochemical reactions of pure indium with Li and Na: anomalous electrolyte decomposition, benefits of FEC additive, phase transitions and electrode performance. *J. Power Sources* **248**, 1105–1117 (2014).
189. Baggetto, L., Marszewski, M., Gorka, J., Jaroniec, M. & Veith, G. M. AlSb thin films as negative electrodes for Li-ion and Na-ion batteries. *J. Power Sources* **243**, 699–705 (2013).
190. Baggetto, L., Allcorn, E., Manthiram, A. & Veith, G. M. Cu_2Sb thin films as anode for Na-ion batteries. *Electrochem. Commun.* **27**, 168–171 (2013).
191. Baggetto, L., Allcorn, E., Unocic, R. R., Manthiram, A. & Veith, G. M. Mo_3Sb_7 as a very fast anode material for lithium-ion and sodium-ion batteries. *J. Mater. Chem. A* **1**, 11163–11169 (2013).
192. Koo, B. *et al.* Intercalation of sodium ions into hollow iron oxide nanoparticles. *Chem. Mater.* **25**, 245–252 (2013).
193. Alcántara, R., Jaraba, M., Lavela, P. & Tirado, J. L. $NiCo_2O_4$ spinel: first report on a transition metal oxide for the negative electrode of sodium-ion batteries. *Chem. Mater.* **14**, 2847–2848 (2002).
194. Su, D., Wang, C., Ahn, H. & Wang, G. Octahedral tin dioxide nanocrystals as high capacity anode materials for Na-ion batteries. *Phys. Chem. Chem. Phys.* **15**, 12543–12550 (2013).
195. Yu, D. Y. W. *et al.* High-capacity antimony sulphide nanoparticle-decorated graphene composite as anode for sodium-ion batteries. *Nat. Commun.* **4**, 2922 (2013).
196. Zhu, C., Mu, X., van Aken, P. A., Yu, Y. & Maier, J. Single-layered ultrasmall nanoplates of MoS_2 embedded in carbon nanofibers with excellent electrochemical performance for lithium and sodium storage. *Angew. Chem. Int. Ed. Engl.* **53**, 2152–2156 (2014).
197. Fullenwarth, J., Darwiche, A., Soares, A., Donnadieu, B. & Monconduit, L. NiP_3: a promising negative electrode for Li- and Na-ion batteries. *J. Mater. Chem. A* **2**, 2050–2059 (2014).
198. Kim, Y. *et al.* Tin phosphide as a promising anode material for Na-ion batteries. *Adv. Mater.* **26**, 4139–4144 (2014).
199. Hong, S. Y. *et al.* Charge carriers in rechargeable batteries: Na ions versus Li ions. *Energy Environ. Sci.* **6**, 2067–2081 (2013).
200. Deng, W. *et al.* A low cost, all-organic Na-ion battery based on polymeric cathode and anode. *Sci. Rep.* **3**, 2671 (2013).
201. Park, Y. *et al.* Sodium terephthalate as an organic anode material for sodium ion batteries. *Adv. Mater.* **24**, 3562–3567 (2012).
202. Hwang, J.-Y. *et al.* Radially aligned hierarchical columnar structure as a cathode material for high energy density sodium-ion batteries. *Nat. Commun.* **6**, 6865 (2015).
203. Aurbach, D. *et al.* Progress in rechargeable magnesium battery technology. *Adv. Mater.* **19**, 4260–4267 (2007).
204. Yoo, H. D. *et al.* Mg rechargeable batteries: an on-going challenge. *Energy Environ. Sci.* **6**, 2265–2279 (2013).
Progress in rechargeable Mg batteries since the original prototype work are reviewed in this article, which focuses on the development of electrolyte solutions and cathode materials.
205. Gregory, T. D., Hoffman, R. J. & Winterton, R. C. Nonaqueous electrochemistry of magnesium: applications to energy storage. *J. Electrochem. Soc.* **137**, 775–780 (1990).
206. Aurbach, D. *et al.* Prototype systems for rechargeable magnesium batteries. *Nature* **407**, 724–727 (2000).
207. Pour, N., Gofer, Y., Major, D. T. & Aurbach, D. Structural analysis of electrolyte solutions for rechargeable Mg batteries by stereoscopic means and DFT calculations. *J. Am. Chem. Soc.* **133**, 6270–6278 (2011).
208. Doe, R. E. *et al.* Novel, electrolyte solutions comprising fully inorganic salts with high anodic stability for rechargeable magnesium batteries. *Chem. Commun.* **50**, 243–245 (2014).
209. Lv, D. *et al.* A scientific study of current collectors for Mg batteries in $Mg(AlCl_2EtBu)_2$/THF electrolyte. *J. Electrochem. Soc.* **160**, A351–A355 (2013).
210. Zhang, R. *et al.* α-MnO_2 as a cathode material for rechargeable Mg batteries. *Electrochem. Commun.* **23**, 110–113 (2012).
211. Imamura, D., Miyayama, M., Hibino, M. & Kudo, T. Mg intercalation properties into V_2O_5 gel/carbon composites under high-rate condition. *J. Electrochem. Soc.* **150**, A753–A758 (2003).
212. Nam, K. W. *et al.* The high performance of crystal water containing manganese birnessite cathodes for magnesium batteries. *Nano Lett.* **15**, 4071–4079 (2015).
213. Liang, Y. *et al.* Rechargeable Mg batteries with graphene-like MoS_2 cathode and ultrasmall Mg nanoparticle anode. *Adv. Mater.* **23**, 640–643 (2011).
214. Liu, B. *et al.* Rechargeable Mg-ion batteries based on WSe_2 nanowire cathodes. *ACS Nano* **7**, 8051–8058 (2013).
215. Orikasa, Y. *et al.* High energy density rechargeable magnesium battery using earth-abundant and non-toxic elements. *Sci. Rep.* **4**, 5622 (2014).
216. Lukatskaya, M. R. *et al.* Cation intercalation and high volumetric capacitance of two-dimensional titanium carbide. *Science* **341**, 1502–1505 (2013).
217. Levi, M. D. *et al.* Solving the capacitive paradox of 2D MXene using electrochemical quartz-crystal admittance and *in situ* electronic conductance measurements. *Adv. Energy Mater.* **5**, 1400815 (2015).
218. Wang, R. Y., Wessells, C. D., Huggins, R. A. & Cui, Y. Highly reversible open framework nanoscale electrodes for divalent ion batteries. *Nano Lett.* **13**, 5748–5752 (2013).
219. Mizuno, Y. *et al.* Electrochemical Mg^{2+} intercalation into a bimetallic CuFe Prussian blue analog in aqueous electrolytes. *J. Mater. Chem. A* **1**, 13055–13059 (2013).

220. Gaddum, L. W. & French, H. E. The electrolysis of Grignard solutions. *J. Am. Chem. Soc.* **49**, 1295–1299 (1927).
221. Kim, H. S. *et al.* Structure and compatibility of a magnesium electrolyte with a sulphur cathode. *Nat. Commun.* **2**, 427 (2011).
222. Guo, Y.-s. *et al.* Boron-based electrolyte solutions with wide electrochemical windows for rechargeable magnesium batteries. *Energy Environ. Sci.* **5**, 9100–9106 (2012).
223. Shterenberg, I. *et al.* Evaluation of $(CF_3SO_2)_2N^-$ (TFSI) based electrolyte solutions for Mg batteries. *J. Electrochem. Soc.* **162**, A7118–A7128 (2015).
224. Mohtadi, R., Matsui, M., Arthur, T. S. & Hwang, S.-J. Magnesium borohydride: from hydrogen storage to magnesium battery. *Angew. Chem. Int. Ed. Engl.* **51**, 9780–9783 (2012).
225. Carter, T. J. *et al.* Boron clusters as highly stable magnesium-battery electrolytes. *Angew. Chem. Int. Ed. Engl.* **53**, 3173–3177 (2014).
226. Tutusaus, O. *et al.* An efficient halogen-free electrolyte for use in rechargeable magnesium batteries. *Angew. Chem. Int. Ed. Engl.* **54**, 7900–7904 (2015).

Acknowledgements
J.W.C. thanks J. Min for his help in the volumetric-energy-density evaluation. J.W.C. acknowledges the support of the National Research Foundation of Korea (NRF) grant funded by the Korea government (MEST) (NRF-2012-R1A2A1A01011970 and NRF-2014R1A4A1003712). D.A. acknowledges help from the Israel Science Foundation, in the framework of the INREP project. This work was also made possible by NPRP grant #5-569-2–232 from the Qatar National Research Fund (a member of the Qatar Foundation).

Competing interests statement
The authors declare no competing interests.

FURTHER INFORMATION

Global Market for Li-Ion Batteries Report 2014–2020: http://www.marketresearch.com/product/sample-8323376.pdf
The Tesla Battery Report: http://www.totalbatteryconsulting.com/industry-reports/Tesla-report/Extract-from-the-Tesla-battery-report.pdf

SUPPLEMENTARY INFORMATION

See online article: S1 (table) | S2 (table) | S3 (table) | S4 (table) | S5 (table) | S6 (table) | S7 (table) | S8 (table) | S9 (table) | S10 (table) | S11 (table) | S12 (table) | S13 (table) | S14 (table) | S15 (table) | S16 (table) | S17 (table) | S18 (table)